Trends of ground-level O_3 in Monterrey, Mexico during 1993-2014: Comparison of with Mexico City and Guadalajara

Iván Y. Hernández Paniagua[1], Kevin C. Clemitshaw[2], and Alberto Mendoza[1,*]

[1]Escuela de Ingeniería y Ciencias, Tecnologico de Monterrey, Campus Monterrey, Av. Eugenio Garza Sada 2501, Monterrey, N.L., México, 64849.
[2]Department of Earth Sciences, Royal Holloway University of London, Egham, Surrey TW20 0EX, UK.
*Corresponding author: mendoza.alberto@itesm.mx

Keywords
Air quality, emissions inventory, time series, wind-sector analysis

Abstract
In developed countries, long-term trends in O_3 have been studied extensively. However, there has been relatively little focus on economically developing countries with significant emissions of pollutant precursors. Here, the dominant role of primary emissions on regional/urban O_3 mixing ratios in Mexico is addressed. High-precision and high-frequency UV-photometric measurements of ambient O_3 have been made since 1993 at 5 sites within the Monterrey metropolitan area (MMA), in NE Mexico. The data sets exhibit variations on time-scales of hours, days, months and years. The O_3 diurnal cycles vary with the length of daylight, which influences photochemical processes that produce O_3. No differences are observed in the amplitudes of the diurnal cycle (AV_d) during weekdays when fossil fuel use and combustion process are higher than during weekends, although the largest AV_d are observed at sites downwind of industrial areas. During weekdays, cycle troughs and peaks are typically recorded at 07:00 and 14:00 CDT, respectively, and during weekends, at 06:00 and 13:00 CDT, respectively.

The O_3 seasonal cycles are driven by the temporal variation of meteorological conditions, with maximum O_3 mixing ratios recorded in spring and minimum values in winter. The largest amplitudes of the seasonal cycles (AV_s) are typically recorded downwind of urban areas, whereas the lowest values are recorded in highly populated areas and close to industrial areas. At all sites, AV_s declined during 1993-1998, followed by persistent increases from 1998 to 2014. Wind sector analysis shows that, at all sites, the highest mixing ratios are recorded from the E and SE sectors, while the lowest ones are recorded in air masses from the W and NW. The wind sector analysis of mixing ratios of O_3 precursors revealed that the dominant sources of emissions are located in the industrial regions within the MMA and the surrounding area. At all sites, the largest annual increases in O_3 are for the E and SE sectors, 0.50 and 0.66 ppb yr^{-1}, respectively, and for the upper data distribution, 0.39-0.75 ppb yr^{-1}. Overall, during 1993 to 2014, within the MMA, O_3 has increased at an average rate of 0.20 ppb yr^{-1} (p<0.001), which is in marked contrast with the large decline of 0.71 ppb yr^{-1} (p<0.001) observed in the Mexico City metropolitan area (MCMA)

for the same period. No clear trend is observed during 1996 to 2014 within the Guadalajara metropolitan area (GMA).

1. Introduction

O_3 is a secondary air pollutant formed in the troposphere via the photo-oxidation of CO, methane (CH_4) and volatile organic compounds (VOCs) in the presence of NO and NO_2 ($NO + NO_2 = NO_x$) (Jenkin and Clemitshaw, 2000). The system of O_3 production is not linear, being VOC-limited whether it responds to the input of VOCs, or NO_x-limited, whether O_3 production increases in response to increasing NO_x emissions (Monks et al., 2015; Pusede et al., 2015). Tropospheric O_3 is of concern to policy makers due to its adverse impacts on human health, agricultural crops and vegetation, and its role as a greenhouse gas despite its relatively short lifetime of around 22.3 ± 3.0 days (Stevenson et al., 2006; IPCC, 2013; WHO, 2014; Lelieveld et al., 2015). As the predominant source of $OH^{\bullet}$, tropospheric O_3 controls the lifetime of CH_4, CO, VOCs, among many other air pollutants (Revell et al., 2015). In polluted regions, increased levels of O_3 are common during seasons with stable high-pressure systems and intense photochemical processing of NO_x and VOCs (Dentener et al., 2005; Xu et al., 2008) and, to lesser extent, downward transport from the stratosphere (Wang et al., 2012). By contrast, the main removal processes for tropospheric O_3 are photolysis and reaction with NO (Atkinson, 2000; Jenkin and Clemitshaw, 2000).

Tropospheric O_3 increased in the Northern Hemisphere (NH) during 1950-1980s due to a rapid increase of precursor emissions derived from the industrialisation and economic growth in Europe and North America (NA) (Staehelin and Schmid, 1991; Guicherit and Roemer, 2000). Since the 1990s, reductions in O_3 precursor emissions in economically developed countries have resulted in decreases in tropospheric O_3 levels (Schultz and Rast, 2007; Butler et al., 2012; Pusede et al., 2015), however, in some regions, increases in O_3 have also been reported. For instance, a substantial study of O_3 data recorded at 158 rural background monitoring stations in Europe carried out by Wilson et al. (2012) showed significant positive annual trends in O_3 annual averages during 1996-2005 at 54 % of the sites, with an average overall increase of 0.16 ± 0.02 ppb yr^{-1}. Positive trends typically corresponded to sites in central and north-western Europe, with negative trends observed at 11 % of the sites, which were located mostly in eastern and south-western Europe. It was concluded that long-term trends of ambient O_3 related to reductions in NO_x and VOC were masked by factors such as changes in meteorology, background O_3 and source patterns of O_3. Similarly, from an analysis of O_3 data from 179 urban sites over France during 1999-2012, Sicard et al. (2016) reported an increasing trend in the annual averages of 0.14 ± 0.19 ppb yr^{-1}, and in the medians of 0.13 ± 0.22 ppb yr^{-1}, attributed to long-range transport and reduced O_3 titration by NO due to reductions in local NO_x emissions. However, Sicard et al. (2016) also reported during the same period that at 61 rural sites, O_3 decreased in the annual averages by 0.12 ± 0.21 ppb yr^{-1}, and in the medians by 0.09 ± 0.22 ppb yr^{-1}.

In the US and Canada, O_3 levels have decreased substantially since 1990s derived from the introduction of air quality policies. For example, in the Greater Area of Toronto during 2000 to 2012, O_3 levels decreased at urban sites by approximately 0.4 % yr^{-1}, and at sub-urban sites by approximately 1.1 % yr^{-1}, as a consequence of a reduction in the mid-day averages of NO_2 of 5.8-6.4 % yr^{-1}, and in the VOC reactivity of 9.3% yr^{-1} (Pugliese et al., 2014). In the US, NO_x and VOCs emissions decreased at national scale during 1980-2008 by approximately 40 % and 47 %, respectively (EPA, 2009; Xing et al., 2013). Lefohn et al. (2010) reported that from 1980 to 2008, the O_3 US EPA exposure metrics of the annual 2nd highest 1-h average, and the annual 4th highest daily maximum 8-h average, decreased at 87 % and 71 % of monitoring sites, respectively, located in 12 US major metropolitan areas, but the lower- and mid-O_3 mixing ratios increased derived from decreased reaction with NO. More recently, Simon et al. (2015) assessed changes in the 1-h average O_3 mixing ratios at around 1400 sites across the US between 1998-2013, using the 5th, 25th, 50th 75th 95th percentiles, and the maximum daily 8-h average. Overall, Simon et al. (2015) observed increases at the lower end of the O_3 data distribution of 0.1-1 ppb yr^{-1}, mostly in urban and sub-urban areas, whereas O_3 decreased at the upper end of the data distribution between 1-2 ppb yr^{-1} at less urbanised areas. Such changes were associated with the implementation of control strategies within the US to abate peak O_3 mixing ratios.

In Mexico, studies of long-term trends in O_3 have focused mostly in the Mexico City Metropolitan Area (MCMA) (Molina and Molina, 2004; Jaimes et al., 2012; Rodriguez et al., 2016), and report a decrease of ca. 33 % during the last two decades (Parrish et al., 2011; SEDEMA, 2016a). By contrast, O_3 has received relatively less consideration at other large metropolitan areas, where Mexican air quality standards are frequently exceeded (Table 1). For instance, official reports indicate that since 2000, ground-level O_3 at the Guadalajara metropolitan area (GMA, the second most populated city) and the Monterrey metropolitan area (MMA, the third most populated city), has breached the 1-h average standard of 110 ppb O_3 by up to 80 %, and the 8-h running average standard of 80 ppb O_3 by up to 50 % (INE, 2011; SEMARNAT, 2015). To date, only Benítez-García et al. (2014) have addressed the changes in ambient O_3 at the GMA and MMA from 2000 to 2011, reporting an increase in O_3 annual averages of around 47 % and 42 %, respectively. However, Benítez-García et al. (2014) did not provide an explanation for the reported trends in O_3, which were determined using non-robust, simple linear regression analysis.

To improve air quality, the Mexican government has introduced several initiatives to reduce primary pollutants emissions. Data from the National Emissions Inventories (NEI) suggest that from 1999 to 2008, anthropogenic NO_x emissions decreased at the MCMA by 3.8 % yr^{-1}, but increased at the GMA and the MMA by 1.9 % yr^{-1}, and by 4.0 % yr^{-1}, respectively; whereas anthropogenic emissions of VOCs decreased at the MMA by 0.2 % yr^{-1}, but increased at the MCMA and the GMA by 2.7 % yr^{-1} and by 3.2 % yr^{-1}, respectively (Fig. S1) (SEMARNAT, 2006, 2011, 2014). However, studies have shown large uncertainties in the NEI data. For instance, the NEI NO_x emission estimates agree with the decrease of

1.7 % yr^{-1} in the NO_2 vertical column density during 2005-2014 for the MCMA reported by Duncan et al. (2016), but disagree for the GMA and the MMA where decreases of 2.7 % yr^{-1} and of 0.3 % yr^{-1}, respectively, are reported. In a previous study, Boersma et al. (2008) observed that NO_x emissions over Mexico derived from NO_2 satellite observations were higher by a factor of 1.5-2.5 times than bottom-up emission estimates, which were lower by 1.6-1.8 times than data reported in the NEI 1999-base year. As well as the NEI, emission inventories have been developed for the MCMA and the MMA by the local governments (SDS, 2015), although only for the MCMA with a frequency of two years since 1996 (SEDEMA, 1999, 2001, 2003, 2004, 2006, 2008, 2010, 2012, 2014, 2016a).

The accuracy of the MCMA emission inventories has been also assessed during several field campaigns. For instance, during the MCMA 2002-2003 campaign, Velasco et al. (2007) observed an overestimation in the 1998 inventory for VOCs emission of alkenes and aromatics, but an underestimation in the contribution of some alkanes. By contrast, for the MCMA 2002 inventory, Lei et al. (2007) reported an underestimation in the VOCs total emissions of around 65 %, based on a simulation of an O_3 episode in 2003 within the MCMA. Therefore, since the emission inventories data are used to predict future air quality, and to design clean air policies, it is imperative to examine the current results of the policies implemented to abate emissions of O_3 precursors. Moreover, the discrepancies between estimates of O_3 precursor emissions and measured data highlight the importance of analysing the long-term trends in O_3 within large metropolitan areas of Mexico.

This study analyses long-term trends in O_3 within the MMA, based on health-based exposure metrics. Long-term and high-frequency measurements of O_3 were recorded at 5 air quality monitoring stations evenly distributed within the MMA from 1993 to 2014. The data sets contain features representative of industrial, urban-background and urban monitoring sites, which allow assessment of O_3 trends and dynamics, pollutant emissions and their contribution to the atmospheric composition depending on local meteorology and air mass transport. In order to better assess photo-chemical production of O_3, total oxidants defined as ($[O_x] = [O_3] + [NO_2]$) were also considered, as O_x is not affected by the titration of O_3 with NO. Additionally, diurnal, seasonal and annual cycles of O_3 and O_x were evaluated in order to interpret the variations observed. The influence of air mass origin on O_3 annual growth rates has also been evaluated. Finally, long-term trends in O_3 and precursor emissions are compared with those observed within the MCMA and GMA.

2. Methodology

2.1 Monitoring of O_3 in the Monterrey Metropolitan Area (MMA).

The MMA (25°40'N, 100°20'W) is located around 720 km N of Mexico City, some 230 km S of the US border in the State of Nuevo Leon (Fig. 1a). It lies at an average altitude of 500 m above sea level (m asl) and is surrounded by mountains to the S and W, with flat terrain to the NE (Fig. 1b). The MMA covers an area of around 4,030 km^2, is the largest urban area in Northern Mexico, and is the third most populous

in the country with 4.16 million inhabitants, which in 2010, comprised 88 % of the population of Nuevo Leon State (INEGI, 2010). The MMA is the second most important industrial area with the highest gross domestic product per capita in Mexico (Fig. 1c). Although the weather rapidly fluctuates on a daily time-scale, the climate is semi-arid with an annual average rainfall of 590 mm, and an annual average temperature of 25.0°C with hot summers and mild winters (ProAire-AMM, 2008; SMN, 2016).

Tropospheric O_3, 6 additional air pollutants (CO, NO, NO_2, SO_2, PM_{10}, and $PM_{2.5}$) and 7 meteorological parameters (wind speed (WS), wind direction (WD), temperature (Temp), rainfall, solar radiation (SR), relative humidity (RH) and pressure) have been monitored continuously, with data summarised as hourly averages, since November 1992 at 5 stations that form part of the Integral Environmental Monitoring System (SIMA) of the Nuevo Leon State Government (Table 2; SDS, 2016). From November 1992 to April 2003, and in accordance with EPA, EQOA-0880-047, Thermo Environmental Inc. (TEI) model 49 UV photometric analysers were used to measure O_3 with stated precision less than ±2 ppb O_3 and a detection limit of 2 ppb O_3. Similarly, in accordance with RFNA-1289-074, TEI model 42 NO-O_3 chemiluminescence detectors were used to measure NO-NO_2-NO_x with stated precision less than ±0.5 ppb NO, and a detection limit of 0.5 ppb NO. In May 2003, replacement TEI model 49C O_3 and model 42C NO-NO_2-NO_x analysers were operated as above, with stated precision better than ±1 ppb O_3 and ±0.4 ppb NO, respectively, and detection limits of 1 ppb O_3 and 0.4 ppb NO, respectively. To rule out instrumentation influences on the determined air pollutants trends, long-term trends based on annual averages were compared with those derived using 3-yr running averages, in accordance with Parrish et al. (2011) and Akimoto et al. (2015) (Supplementary Information S1.1; Fig. S2). Calibration, maintenance procedures and quality assurance/quality control (QA/QC) followed protocols established in the Mexican standards NOM-036-SEMARNAT-1993 and NOM-156-SEMARNAT-2012. The SIMA dataset has been validated by the Research Division of Air Quality of the Secretariat of Environment and Natural Resources (SEMARNAT). The monitoring of O_3 and other air pollutants at the MCMA and the GMA is detailed in the Supplementary Information S1.2-3.

2.2 NEI data

Estimates of NO_x and VOCs emissions have been made at the national scale for the 1999-, 2005- and 2008-base years and reported in the NEI, and were obtained from the SEMARNAT website (http://sinea.semarnat.gob.mx). The data set is provided by emission source (mobile, point, area and natural), air pollutant, and at national, state and municipality scales. The NEI emission estimates are developed in accordance with the Manual for the Emission Inventories Program of Mexico (Radian, 2000), which is based on the US EPA AP-42 emission factors categorisation (EPA, 1995). The emission factors are regionalised for each Mexican state, based upon on-site measurements and survey information. Updates to the emission factors have been conducted for each released NEI, although no changes in the methodology were implemented between the 1999- and 2008-base years. Overall, the mobile emissions were estimated using the MOBILE6-Mexico model (EPA, 2003). The emissions from

point sources were derived using the annual operation reports submitted to the Environment Ministry. The emissions from area sources were obtained using the categorisation of Mexican area sources and the regionalised AP-42 emission factors.

The MCMA emissions inventories have been developed with a 2-year frequency since 1996, and were obtained from the MCMA Environment Secretariat website (http://www.aire.cdmx.gob.mx/). The methodology used to construct the MCMA inventories estimates is consistent with that used in the NEI (SEDEMA, 2016a), which is based on the AP-42 EPA emission factors. However, more speciated emission factors have been developed in each released version, considering updates in the local industrial activity, survey information and field measurement campaigns. To date, the only significant change in the methodology is the replacement of the Mobile6-Mexico model with the MOVES model to obtain the 2014-base year mobile emissions (SEDEMA, 2016b). As for the MCMA inventories, more speciated emission factors than those contained in the NEI were developed to produce the MMA emissions inventory 2013-base year (SDS, 2015), although, mobile emissions estimates were obtained with the Mobile6-Mexico model (EPA, 2003).

2.3 Analysis of data

SIMA, SIMAT (Atmospheric Monitoring System of the MCMA) and SIMAJ (Atmospheric Monitoring System of the GMA) instrumentation recorded O_3 data every minute, which were then validated and archived as 1-h averages. Total SIMA O_3 data capture by year and site are shown in Fig. S3. Data capture averaged during 1993-2014 ranged from 82.6 % at GPE to 93.3 % at SNB, with data capture <50 % during 1998-2000 at GPE, in 1998 at SNN, and in 1999 at OBI. A threshold of 75% data capture was defined to consider data valid and representative (ProAire-AMM, 2008; Zellweger et al., 2009; Wilson et al., 2012). All data were processed with hourly averages used to determine daily averages, which were used to calculate monthly averages, from which yearly averages were obtained.

The SIMA, SIMAT and SIMAJ O_3 data sets were analysed extensively using the *openair* package v. 1.1-4 (Carslaw and Ropkins, 2012) for R software v. 3.1.2 (R Core Team, 2013). In this study, the *openair* functions windRose, timeVariation and TheilSen were used to analyse air pollution data. Briefly, the windRose summarises wind speed and wind direction by a given time-scale, with proportional paddles representing the percentage of wind occurrence from a certain angle and speed range. The timeVariation function was used to obtain normalised daily cycles by season, and weekly cycles, with the 95 % confidence intervals in the cycles calculated from bootstrap re-sampling, which accounts for better estimations for non-normally distributed data (Carslaw, 2015). Finally, long-term trends of air pollutants at the MCMA, GMA and MMA were computed with the TheilSen function, which is based on the non-parametric Theil-Sen method (Carslaw, 2015; and references therein). The Theil-Sen estimate of the slope is the median of all slopes calculated for a given n number of x,y pairs, while the regression

parameters, confidence intervals and statistical significance are determined through bootstrap re-sampling. It yields accurate confidence intervals despite the data distribution and heteroscedasticity, and is also resistant to outliers.

The trends computed with *openair* were contrasted with those calculated using the MAKESENS 1.0 macro (Salmi et al., 2002) as follows. Firstly, the presence of a monotonic trend (increasing or decreasing) was tested with the non-parametric Mann-Kendal test. For the MCMA, GMA and MMA the available yearly data are n>10, hence positive values in the Z parameter correspond to positive trends and vice versa for negative values of Z. The significance of the estimated trend was tested at α=0.001, 0.01, 0.05 and 0.1 using a two-tailed test. Secondly, slopes of linear trends are calculated with the non-parametric Sen's method. The Sen's method assumes linear trends, with a Q slope and a B intercept. To calculate Q, first the slopes of all data values are calculated in pairs, with the Sen's estimator slope as the median of all calculated slopes. Finally, 100(1-α) % two-sided confidence intervals about the slope estimate are obtained based on a normal distribution. The comparison of estimated trends from both approaches is shown in the Supplementary information S1.4 (Fig. S4).

The O_3 and other air pollutants time-series were decomposed into trend, seasonal and residual components using the Seasonal-Trend Decomposition technique (STL; Cleveland et al., 1990). STL consists of two recursive procedures: an inner loop nested inside an outer loop, assuming measurements of x_i (independent) and y_i (dependent) for i = 1 to n. The seasonal and trend components are updated once in each pass through the inner loop; each complete run of the inner loop consists of $n_{(i)}$ such passes. Each pass of the outer loop consists of the inner loop followed by a computation of the robustness weights, which are used in the following run of the inner loop to minimise the influence of transient and aberrant behaviour on the trend and seasonal components. The initial pass of the outer loop is performed with all robustness weights equal to 1, followed by $n_{(0)}$ passes of the outer loop. The Kalman Smoother (KS) was used to provide minimum-variance, unbiased linear estimations of observations and to impute missing data to satisfy the STL (Reinsel, 1997; Durbin et al., 2012; Carslaw, 2015). Overall, statistical seasonal auto-regressive and moving averages with annual seasonal components were employed. Statistical analyses were carried out with SPSS 19.0.

In order to carry out seasonal analyses of data, seasons were defined according to temperature records in the NH, as described previously (Hernandez-Paniagua et al., 2015): winter (December-February), spring (March-May), summer (June-August) and autumn (September-November). Wind-sector analyses of data were performed by defining 8 wind sectors each of 45° starting from 0° ± 22.5°. The lower bound of each sector was established by adding 0.5° to avoid data duplicity. Data were assigned to a calm sector when wind speed was ≤ 0.36 km h^{-1}. To assess regional transport, air mass back-trajectories (AMBT) were calculated using the HYSPLIT model v.4 (NOAA Air Resources Laboratory (ARL); Stein et al., 2015), with the Global NOAA-NCEP/NCAR reanalysis data files on a latitude-longitude grid of 2.5

degrees, downloaded from the NOAA ARL website (http://ready.arl.noaa.gov/HYSPLIT.php). HYSPLIT frequency plots of 96-h AMBT were constructed for every 6 h during the year 2014 with an arrival altitude of 100 m above ground level.

3. Results and Discussion

3.1 Wind occurrence at the MMA

The MMA is highly influenced by anti-cyclonic, easterly air masses that arrive from the Gulf of Mexico, especially during summer (Fig. S5). Figure 2 shows the frequency count of 1-h averages of wind direction by site and season within the MMA during 1993-2014. At all sites, apart from OBI, the predominant wind direction is clearly E, which occurs between 35-58 % of the time depending on season. These air masses are augmented by emissions from the industrial area E of the MMA, which are transported across the urban core and prevented from dispersing by the mountains located S-SW of the MMA. On average, the highest wind speeds are observed during summer. By contrast, calm winds of ≤ 0.36 km h^{-1} (0.1 m s^{-1}) occurred less than 2 % of the time at all sites, most frequently in winter, and least frequently in summer.

3.2 Continuous records and trend of daily maxima of O_3 and O_x

Figure 3 shows the complete data set of 1-h averages of O_3 recorded at the 5 monitoring stations within the MMA from January 1993 to December 2014. The highest O_3 1-h average was observed at SNB, and is likely to arise from short-range transport and large upwind emissions of O_3 precursors from vehicles and industries. The highest O_3 mixing ratios (1-h averages) are typically observed in April (spring), with lowest values usually recorded in December and January (winter) (Fig. 3). Table S1 summarises the minimum, maximum, mean (average) and median hourly O_3 mixing ratios recorded. The highest mixing ratios recorded were 186 ppb O_3 at GPE in 1997, 146 ppb O_3 at SNN in 2004, and 224 ppb O_3 at SNB in 2001. At OBI and STA, the highest O_3 mixing ratios were both recorded on June 2, 1993: 182 ppb at 12:00 CDT at OBI, and 183 ppb at 13:00 CDT at STA. Annual averages varied from 14 ± 14 ppb O_3 at OBI in 2001 to 32 ± 23 ppb O_3 at SNB in 1993, whereas annual medians ranged from 10 ppb O_3 at OBI in 2001 to 28 ppb O_3 at SNN in 1993.

Reaction with O_3 rapidly converts NO to NO_2, and therefore mixing ratios of odd oxygen ($O_x = O_3 + NO_2$) were calculated for each hour during 1993-2014 at the 5 sites within the MMA (Table S2; Fig. S6). Minimum values of O_x ranged from 2 ppb, observed at all sites mostly during the whole studied period (except for 1993,1997, 2005, 2009 and 2013 and 2014) to 13 ppb at OBI in 2007. Maximum values of O_x ranged from 99 ppb at SNN in 2002, to 330 at OBI in 1993. Annual averages varied from 23 ± 17 ppb at SNN in 2002 to 51 ± 27 ppb at OBI and at STA in 2001 and 2006, respectively, whereas annual medians ranged from 21 ppb at SNB and SNN, in 2001 and 2002, respectively, to 46 ppb at OBI and STA in 2001 and 2006, respectively. The highest values of O_x were observed at OBI during 1993-2002, which coincided with the largest mixing ratios of NO_2 that were likely dominated by vehicle emissions. Since 2003, the highest O_x mixing ratios recorded at STA were likely due to increase upwind NO_x and

VOCs emissions mostly from nearby industries (SEMARNAT, 2006, 2011, 2014; SDS, 2015). As for O_3, O_x exhibits a seasonal cycle with the highest values in spring and lowest values in winter.

A study conducted among asthmatic children resident in the MCMA revealed an increase in coughing and wheezing rates, associated with cumulative exposure to high 1-h averages mixing ratios of O_3 and NO_2 (Escamilla-Nuñez et al., 2008). To assess changes in cumulative exposure to O_3 and O_x within the MMA, long-term trends of de-seasonalised maximum daily 1-h averages in O_3, O_x and NO_x were calculated, using annual averages filtered with the STL technique (Fig. 4). Overall, the maximum daily O_3 1-h averages show significant increasing trends ($p<0.05$) of 0.35 to 0.79 ppb O_3 yr^{-1} at GPE and SNN, respectively. The largest annual increase observed at SNN is likely influenced by the significant ($p<0.05$) annual growth of 1.90 ppb y^{-1} in NO_x in levels as shown in Fig. 4, which can be ascribed to localised industrial emissions and constant urban growth W of the MMA (ProAire-AMM, 2008; SDS, 2015). By contrast, the non-significant ($p>0.05$) trend of -0.01 ppb O_3 yr^{-1} observed at STA is may be masked by local import of O_3, combined with air masses stagnation, since NO_x does exhibit a significant ($p<0.05$) annual increase of 1.59 ppb yr^{-1}. However, long-term monitoring of VOCs trends and sources is needed to determine the origin of the no trend current status at STA.

The maximum daily 1-h mixing ratios of O_x show significant increasing trends ($p<0.1$) of 0.18, 0.62 and 0.43 ppb O_x yr^{-1} at GPE, SNN and SNB, respectively, which arise either from an increment in NO_x or O_3 levels as shown in Fig. 4. By contrast, significant decreasing trends ($p<0.05$) of 0.49 and 0.56 ppb O_x yr^{-1} are seen at OBI and STA, respectively. For OBI, the negative O_x trend is likely due to the decreasing levels of NO_x, as result of improved exhaust catalyst technology in an expanding fleet of new vehicles and less traffic loading because the population is moving out of the MMA core (INEGI, 2015; SDS, 2015). At STA, the negative trend in O_x contrasts with the significant increase in NO_x, and the no trend status in O_3. This could be due to the arrival at OBI and at STA of chemically processed air masses with decreased VOC/NO_x ratios, compared with those arriving at SNN loaded with fresh emissions from the nearby industrial area.

3.2 O_3 daily cycles

Figure 5 shows daily profiles of O_3, O_x, NO, NO_2, NO_x, and SR averaged over the 5 sites within the MMA. O_3 generally dips during rush hour by reaction with NO, which occurs around 07:00 in spring and summer and 08:00 in autumn and winter; the 1-h difference in the dip derives from the change to daylight saving time during spring and summer. O_3 generally peaks around 13:00 in spring, 12:00 in summer (co-incident with SR), and about 14:00 in autumn and winter. Similar profiles are observed for O_3 being in an anti-phase cycles of NO_2 mixing ratios (r=0.93 (winter) to 0.97 (summer) ($p<0.05$), in all seasons). Despite differences of 1 to 3 hours in the timing of the O_3 dips and peaks as shown in Fig. 5, they coincide broadly with those observed at urban areas in NA and in the NH. For example, O_3 daily maxima occur between 13:00 and 15:00 in the MCMA (Jaimes-Palomera et al., 2016), in the Los Angeles urban area (VanCuren,

2015), and in the Toronto urban area (Pugliese et al., 2014). Similar timing for O_3 peaks was reported at 4 metropolitan areas in Japan (Akimoto et al., 2015), and in Central London (Bigi and Harrison, 2010).

To compare the O_3 diurnal cycles by season, normalised daily profiles were constructed by subtracting daily averages from hourly averages in order to remove the impact of the long-term trends (Fig. 6; Hernández-Paniagua et al., 2015), with daily amplitude values (AV_d; calculated by subtracting the lowest normalised values from the highest normalised values) used to assess diurnal variations in O_3 among seasons. The lowest AV_d values occur in winter at all sites in response to reduced SR, whereas the largest values observed during summer result from enhanced photochemistry under high SR. The lowest AV_d observed at SNN is associated with the inflow of NE and E air masses laden with fresh emissions of O_3 precursors, which are transported to downwind sites (SNB and STA), and become stagnated by the surrounding mountains. This would explain that the largest AV_ds within the MMA are observed at sites receptor of photochemically processed air masses, particularly STA (Fig. 6). In Toronto, for example, Pugliese et al. (2014) observed that O_3 maxima were enhanced by photochemical processing of air masses from polluted wind sectors, whereas O_3 maxima were decreased in cleaner air masses. O_3 daily profiles and AV_d similar to those for the MMA were observed at Linan in China from 1995 to 2006 (Xu et al., 2008), with variability in AV_d ascribed to increasing emissions of O_3 precursors, particularly NO_x.

The existence of trends in O_3 AV_d during 1993-2014 was tested using de-seasonalised annual averages filtered with STL. The lowest annual AV_d of 18.6 ppb O_3 was observed for OBI in 1995, whereas the largest of 49.5 ppb O_3 was calculated for STA in 2004. Despite their annual variability, significant increasing trends (p<0.05) in AV_d were detected at all sites apart from STA (Fig. 7), and ranged from 0.48 ppb yr^{-1} at GPE to 0.77 ppb yr^{-1} at SNN. These increasing trends in O_3 AV_d agree with annual increments in daily maximum 1-h O_3 averages observed at all sites (Fig. 4), whereas the no trend status at STA is likely related to the lack of trend in the daily maximum 1-h O_3 average. Such increments would imply an increase in the exposure to O_3 of 1.54-3.26 % yr^{-1} in a daily time scale for inhabitants of the MMA (Escamilla-Nuñez et al., 2008). A plausible alternative to reduce the population exposure to O_3 is the reduction of 25-50% in ground-level VOCs within the MMA as proposed by Sierra et al. (2013), which would decrease daily exposure to O_3 by reducing peak O_3 between 0.7-13.4 %.

3.3. O_3 seasonal cycles within the MMA from STL data

Annual variations in ground-level O_3 have been be correlated with the seasonality of temperature, RH and SR (Camalier et al., 2007; Zheng et al., 2007). Hence, the annual average cycle for the above mentioned variables was constructed by averaging monthly averages for the same month during the studied period (Fig. 8a). A linear regression analysis was conducted to test the O_3 mixing ratios dependence to temp., rain, RH and SR, using data from the annual average cycles. The strongest relationship was observed between O_3 and SR (r= 0.72, p<0.001; Fig. S7). To depict the O_3 seasonal

dependence, monthly averages of O_3 and SR for the MMA during 1993-2014 were filtered with the STL technique to obtain the seasonal component (Cleveland et al., 1990). Figure 8b shows the seasonal cycles of O_3, with spring-time maxima and winter minima, in strong correlation with SR (Lelieveld and Dentener, 2000).

This behaviour agrees well with the O_3 spring maxima and winter minima characteristic of the US southeast regions (Strode et al., 2015), and follows the NH mid-latitudes O_3 cyclic pattern (Monks 2000; Vingarzan, 2004). However, it differs with the O_3 seasonal cycles observed over the US west coast regions (particularly in California), where the maxima occur between June-August, in response to the local influence of precursor emissions upon O_3 production and photochemical conditions (Vingarzan, 2004; Strode et al., 2015). By contrast, downward spikes in the seasonal cycles of O_3 within the MMA are observed recurrently between July-August (Fig. 8b), which likely result from high wind speeds (>6 km h^{-1} in average) that disperse O_3 precursors and increase the boundary layer height (ProAire-AMM, 2008), and high day-time temperatures (>40° C) that could suppress the O_3 formation. Steiner et al. (2010) reported that within VOC-limited areas, temperatures >38° C may lead to decreases in O_3 formation, in response to a decrease in the peroxyacetyl nitrate lifetime (NO_x sink). The peak in O_3 observed in September is characteristic of humid regions, and can be ascribed to an increase in OH radicals derived from the increment in RH during the rainy season (Lee et al., 2014). Zheng et al. (2007) reported that this O_3 secondary peak became less noticeable since 2000 over the mid-western and eastern US regions. Indeed, the O_3 secondary peak is characteristic of the Asian summer monsoon, which transports maritime clean air to land with constant rainfall, thereby increasing RH (Xu et al., 2008).

The seasonal amplitude value (AV_s) may provide insights regarding the response in O_3 production to year-to-year variations in the emissions of O_3 precursors and climate. O_3 AV_ss were calculated for the average seasonal cycle within the MMA, as the difference peak-to-trough for each annual cycle after filtering monthly averages with STL, considering the largest value in spring as the peak of the cycle. An average AV_s of 15.1 ± 2.97 (1σ) ppb O_3 was calculated from 1993-2014 within the MMA, with the lowest AV_s of 10.3 ppb O_3 determined in 1998, and the largest value of 19.0 ppb O_3 observed in 2014. AV_s for the MMA are similar to those calculated using dynamic linear models by Zheng et al. (2007), over the mid-western US region between ca. 12 ppb O_3 in 2004 and 18 ppb O_3 in 1999, but lower than those between ca. 19 ppb O_3 in 2004 and 27 ppb O_3 in 1999 determined for the eastern region. When compared with European regions, the AV_s determined within the MMA are slightly lower than those calculated at the North Kensington site in London, which ranged from ca. 7.0 ppb O_3 in 2000 to ~25.5 ppb O_3 in 2005 (Bigi and Harrison, 2010), presumably due to lower emissions of NO_x and VOCs within the MMA (SDS, 2015). It is striking that the average AV_s for the MMA agrees well with that of 10.5 ppb O_3 recorded during 2004-2005 at the Pico Mountain Observatory in Portugal, which is a receptor of exported NA air pollution (Kumar et al., 2013). Thus, despite trends of increasing O_3 precursor emissions within the MMA, AV_s lie

417 within the range of those recorded at sites in the mid-west US, but are slightly lower than those
418 determined for more populated and urbanised sites in the east US and Western Europe.
419
420 Figure 8c shows long-term trends of O_3 AV_s for the 5 monitoring sites within the MMA during 1993-2014,
421 determined as above. Overall, significant decreases (p<0.05) in O_3 AV_s are observed during 1993-1997
422 for GPE and SNB and, during 1993-1998 for SNN, OBI and STA, which ranged from 0.78 ppb O_3 yr^{-1} for
423 GPE to 2.28 ppb O_3 yr^{-1} for SNN (Fig. 8d). By contrast, significant increases (p<0.05) in O_3 AV_s are
424 observed for all sites since 1998, which ranged from 0.9 ppb O_3 yr^{-1} at GPE to 0.75 ppb O_3 yr^{-1} at SNN.
425 It is very likely that the observed decline in O_3 AV_s is ascribed to the economic crisis experienced in
426 Mexico during 1994-1996 (Tiwari et al., 2014; INEGI, 2016), which caused a reduction in VOCs and NO_x
427 emissions from the industrial activity as reflected in the gross domestic product in 1995 (Fig. S8).
428 Moreover, the reported recovery of the economy since 1997 may have driven the increases in precursor
429 emissions leading to the observed increases in O_3 AV_s. During the global economic recession of 2008-
430 2009, Castellanos and Boersma (2012) observed a reduction of 10-30 % in the tropospheric levels of
431 NO_2 over large European urban areas, which is consistent with a faster decline of 8 ±5 % yr^{-1} in the NO_2
432 column density during the same period detected by Russell et al. (2012) at US urban regions. This
433 behaviour may explain the opposite trends determined before and after the economic crisis within the
434 MMA, and that the lowest rates of change in the O_3 AV_s were observed at GPE, which contrasts with the
435 largest ones determined at SNN driven by increases in industrial activity.
436
437 **3.4. Long-term trends of O_3 within the MMA during 1993-2014**
438 Long-term trends of the annual 5th and 95th percentiles (%ile), median and average of O_3 during 1993-
439 2014 were calculated using the Mann-Kendall test and Sen's estimate for the 5 sites within the MMA
440 (Salmi et al., 2002; Carslaw and Ropkins, 2012), and are shown in Fig. 9. The long-term trends were
441 constructed from de-seasonalised annual data derived from monthly averages filtered with STL, which
442 were calculated from daily data of all 1-h averages, as described in Methodology (Sect. 2.3). Overall, O_3
443 shows significant increasing trends (p<0.05) mostly in the annual averages ranging from 0.11 ppb O_3 yr^{-1}
444 at SNB to 0.31 ppb O_3 yr^{-1} at OBI, and in the 95th %ile, which ranged from 0.39 ppb O_3 yr^{-1} at OBI and
445 SNB to 0.75 ppb O_3 yr^{-1} at SNN. The 5th %ile increased significant only at OBI in 0.08 ppb yr^{-1}, while the
446 median increased at SNN by 0.14 ppb O_3 yr^{-1} and at OBI by 0.23 ppb O_3 yr^{-1}. Note that if trends are
447 segmented and considered only after the decline in 1994-1995, the only significant change is that the O_3
448 growth rate at SNN would increase to 0.31 ppb O_3 yr^{-1} and GPE would decrease to 0.14 ppb O_3 yr^{-1},
449 while in the 95th %ile the trends would decline slightly at GPE and SNB to 0.27 ppb O_3 yr^{-1}, and at OBI
450 to 0.42 ppb O_3 yr^{-1}. Despite exhibiting the highest O_3 mixing ratios within the MMA, STA did not exhibited
451 significant trends in any of the tested metrics.
452
453 To gain insights of changes in the O_3 precursor emissions within the MMA during the studied period,
454 long-term trends of NO_x and CO were calculated as above, and are shown in Fig. 10. The increasing

trends at GPE, SNN and SNB are likely caused by increasing emissions of NO_x, which is in agreement with significant increases (p<0.05) in the annual averages of NO_x at those sites, that ranged from 0.19 ppb NO_x yr^{-1} at GPE to 0.51 ppb NO_x yr^{-1} at SNN. The large growth rates both in O_3 and NO_x identified at SNN are likely the result of increased emissions from a growing number of industries and sub-urban development E of the MMA. However, at OBI, the increasing positive trend in O_3 contrasts with the NO_x decreasing trend of 0.40 ppb NO_x yr^{-1}, which may arise from the O_3 production non-linear response in the VOC-sensitive MMA airshed, to increasing emissions of VOCs and decreasing NO_x emissions (Sierra et al., 2013; Menchaca-Torre et al. 2015). Moreover, the decrease in NO_x detected at OBI may reflect the positive results of stricter emissions standards for mobile sources such as the fitting of improved catalyst technology, which may have been offset at the other monitoring sites by emissions from the industrial sources.

When O_x were tested for linear trends, significant (p<0.05) increases of 0.48 ppb O_x yr^{-1} at GPE and of 0.69 ppb O_x yr^{-1} at OBI agree with those of detected in O_3, whereas at STA O_x increased in 0.48 ppb O_x yr^{-1}. At SNN and SNB, the non-significant (p>0.05) trends in O_x contrast with those of O_3 increasing. The largest O_x trend observed at OBI is may be ascribed to decreasing NO_x but increasing VOCs. The NO_x positive trends determined within the MMA are in good agreement with the increase of 7.8 ± 11.2 % in the NO_2 column over the MMA during 2005-2014 reported by Duncan et al. (2016). Moreover, the decreases in NO_x and O_3 observed between 1994-1996 are likely the response to the economic crisis during the same period in Mexico, when the DGP decreased by 5.9 % (Fig. S8). Consistent with economic indicators, annual averaged petrol sales in the Nuevo Leon state in 1995 decreased by 2.4 % in relation to 1994, but increased linearly from 1996 to 2008 at an approximate rate of 98,800 m^3 petrol yr^{-1} (r = 0.90) (Fig. S9) (SENER, 2015). As for petrol sales, registered vehicles in Nuevo Leon show significant variations between 1993-1996, but increase linearly since 1997 at a rate of 100,000 vehicles yr^{-1} (r=0.99).

Data from the MMA Emission Inventories suggest that NO_x emissions from total anthropogenic and mobile sources decreased around 15 % and 8 % from 1995 to 2013, respectively, (SDS, 2015), whereas the NEI data suggest increases from 1999 to 2008 for the same categories of 55 % and 60 %, respectively (Fig. 11a). A large overestimation in the NEI data may be confirmed when compared with the CO data recorded within the MMA during 1993-2014, which exhibited a linear negative trend of 1.8 % yr^{-1}, and disagree with the increases in emission estimates of CO for the 2005- and 2008-base years (Fig. 11b). Similarly, NEI estimates indicates that VOC emissions in 2005 were larger than those in 1999 by 155 %, and those for 2008 are larger than the MMA estimates for 2013 by 255 % (Fig. 11c), suggesting a possible overestimation in the emissions as reported in previous studies (Velasco et al., 2007).

The O_3 trends observed within the MMA for the mid- and upper-data distribution agree with those observed by Simon et al. (2015) from 1998 to 2013 at US western urban areas, but are opposite to those

for southern US urban areas. As for the MMA, the increasing O_3 in urban areas was ascribed to changes in NO_x emissions. Moreover, Simon et al. (2015) attributed increases in the O_3 5th percentile of 0.1-1 ppb yr^{-1} at urban areas to reductions in NO_x emissions, behaviour also reported in central London by Bigi and Harrison (2010) during 1996-2008 and similar to that observed at OBI. O_3 growth rates similar to those recorded within the MMA of 0.22-0.37 ppb O_3 yr^{-1} were recorded at four urban areas in Japan during 1990-2010 (Akimoto et al., 2015), and were ascribed to trans-boundary transport of O_3 and a decrease of the NO tritation effect. By contrast, Sather and Cavender (2016) reported that in 4 South Central US urban areas, the reduction in ambient levels of NO_x and VOCs of 31-70 % and 43-72 %, respectively, resulted in a reduction of 18-37 ppb O_3 in the 8-h averages opposite to the increases observed within the MMA. This highlights the need of long-term VOCs monitoring within the MMA to revise the effectiveness of current air quality policies.

3.5 O_3 growth rates by wind sector within the MMA

Long-term trends in O_3, O_x and NO_x recorded within the MMA were determined by wind sector. Data were split into 8 wind sectors, with the Mann-Kendall test and Sen's estimate used to calculate annual growth rates. Table 3 shows that significant (p<0.05) annual O_3 growth ranged from -0.05 ppb O_3 yr^{-1} for STA and W, to 0.66 ppb O_3 yr^{-1} for OBI and SE. The largest and most significant O_3 growth rates are seen for the E and SE sectors, whereas the lowest significant growth rates correspond to the W sector. Similarly, the largest significant (p<0.05) O_x growth rates of 0.52 ppb O_x yr^{-1}, 0.55 ppb O_x yr^{-1} and 0.78 ppb O_x yr^{-1} at GPE, SNN, and at SNB, respectively are observed for the E and SE sectors (Table S3). By contrast, significant (p<0.05) decreasing trends of 0.48 ppb O_x yr^{-1} and 1.52 ppb NO_x yr^{-1} were calculated for the SW sector at OBI, whereas non-significant (p>0.05) trends were apparent at STA. The observed growth rates highlight the dominant contribution of local industrial emissions of O_3 precursors and the role of regional-scale transport of O_3: largest growth rates are observed at SNN and OBI that are downwind of significant industrial emissions (Table S4).

3.6. Comparison of MMA O_3 weekly profiles with those at MCMA and GMA

Hourly O_3 data were used to construct weekly averaged profiles for the MCMA from 1993 to 2014, and for the GMA from 1996 to 2014. Figure 12 compares weekly O_3 cycles within the MMA with those for the MCMA and GMA. In each case, and consistent with observations in other major NA urban areas, the lowest O_3 mixing ratios occur during the morning rush hour due to O_3 tritation with NO emitted from on-road sources, with peak values apparent after mid-day (Stephens et al., 2008; Jaimes-Palomera et al, 2016). It should be noted that the peak value for the MCMA occurs an hour or so earlier than for the MMA and GMA and is attributed to accelerated photo-chemical production of O_3 during late morning (Volkamer et al., 2010). As might be anticipated, larger AV_d of 76.9 ± 1.6 ppb O_3 were observed for the MCMA than for the GMA (46.1 ± 1.0 ppb O_3) and MMA (37.6 ± 0.4 ppb O_3), and as seen in Fig. 13, appear to be related to the relative emissions of the O_3 precursors.

No significant differences (p>0.05) were observed at any of the metropolitan areas between O_3 AV_d during weekends and weekdays. This lack of a weekend effect in O_3 was reported previously at the MCMA for 1987-2007 by Stephens et al. (2008), who attributed it to weekday O_3 production being limited by VOCs and inhibited by NO_x; this was also observed by Song et al. (2010). By contrast, simultaneous decreases in emissions of VOCs and NO_x mostly from vehicle sources during weekends could have counteracting effects on the O_3 production rates, leading to similar levels of O_3 during weekdays at the 3 metropolitan areas. This behaviour was reported previously by Wolff et al. (2013) for US urban areas of the Northeast, Midwest and Coastal California regions, which exhibited similar or even higher (±5 %) O_3 levels during weekdays than at weekends, despite lower O_3 precursor emissions during weekends. Moreover, Wolff et al. reported that from 1997-1999 to 2008-2010 the sites studied exhibiting a weekend effect decreased from ca. 35 % to less than 5 %, which was attributed to an increase in the VOC/NO_x emission ratio derived from a greater decline in NO_x than in VOCs emissions (Pusede et al., 2014).

It is likely that the O_3 weekly patterns observed at the metropolitan areas arise from reduced traffic activity during weekends, leading to increases in ratios of VOCs/NO_x. Within the MMA, this would be confirmed by lower NO_x mixing ratios (on average 5 %) during weekends, changing to a transition O_3 production between VOC- and NO_x-limited during weekends. Moreover, a change to a NO_x-limited O_3 production derived from the reduction in NO_x seems unlikely since this would result in lower O_3 levels during weekends, not observed at any of the studied urban areas (Torres-Jardon et al., 2004). However, continuous measurements of ambient VOCs levels are required to explain the weekly patterns observed.

3.7. Long-term trends at MCMA, GMA and MMA from 1993 to 2014

De-seasonalised annual averages of O_3, NO_x and CO for sites within the MCMA and GMA were calculated as for the MMA sites. Figure 13 shows long-term trends for these pollutants determined with the Mann-Kendall and Sen's estimate. Within the MMA, a significant (p<0.05) increasing trend of 0.20 ppb O_3 yr^{-1} is observed during 1993-2014, within the MCMA a significant (p<0.05) decreasing trend of 0.71 ppb O_3 yr^{-1} occurred during the same period, while within the GMA, a non-significant (p>0.05) trend of -0.09 ppb O_3 yr^{-1} is evident during 1996-2014. The observed trends in O_3 during the studied period, reflect the response to decreasing NO_x (1.24 ppb yr^{-1}; p<0.05) within the MCMA (Fig. 13a), and increasing NO_x (0.28 ppb yr^{-1}; p<0.05) within the MMA (Fig. 13c). Such changes in tropospheric NO_x of 1.0 % yr^{-1} within the MMA and of -1.24 % yr^{-1} within the MCMA, agree with those reported by Duncan et al. (2016), in the NO_2 column during 2005-2014 over the MMA (0.8 % yr^{-1}) and MCMA (-0.1 % yr^{-1}). The status of no trend in O_3 within the GMA contrasts with the significant decrease in NO_x levels (1.47 ppb yr^{-1}; p<0.05) observed both at ground-level (-2.0 % yr^{-1}) and in the NO_2 column (-0.2 % yr^{-1}).

Long-term trends of de-seasonalised O_3 annual median, 5^{th} and 95^{th} percentiles at the 3 urban areas were determined following the same methodology as for annual averages (Fig. S10). Overall, the linear trends observed in O_3 annual averages for the MMA and MCMA are also seen in the other tested metrics,

with significant (p<0.05) increases at MMA ranging from 0.05 ppb O_3 yr^{-1} (5^{th} percentile) to 0.41 ppb O_3 yr^{-1} (95^{th} percentile), and decreases at MCMA between 0.37 ppb O_3 yr^{-1} (5^{th} percentile) and 2.32 ppb O_3 yr^{-1} (95^{th} percentile). As for the O_3 annual averages, the GMA shows non-significant (p>0.05) trends in the other tested metrics. Notably, only the tropospheric CO decreased significantly (p<0.05) at the 3 urban areas studied, with the largest decrease rate of 0.12 ppm CO yr^{-1} detected at the MCMA and the lowest one of 0.02 ppm CO yr^{-1} calculated at the MMA. Thus, whereas O_3 precursors have decreased linearly within the MCMA and the GMA during the studied period, within the MMA those have increased during the same period despite the introduction of emission control policies (SDS, 2015).

The trends in O_3 observed in this study for the MCMA and MMA, agree with the reduction of 20 ppb O_3 during 1991-2011 for the MCMA reported by Jaimes et al. (2012), and with the reduction of 8 ppb O_3 during 2000-2011 for the MMA reported Benítez-García et al. (2014). However, the no trend status in O_3 within the GMA, is in contrast to the increase of 12 ppb O_3 during 2000-2011 reported by Benítez-García et al. (2014), which is likely due to the different periods assessed in both studies. It seems unlikely that meteorology could obscure the O_3 trends for the GMA determined here (Camalier et al., 2007), since all O_3 data used to construct the long-term trends were filtered out for meteorological effects with the STL technique. The decreases in O_3 reported here for the upper data distribution (0.71-2.32 ppb yr^{-1}) within the MCMA are larger than those reported by Simon et al. (2015) of 1-2 ppb yr^{-1} during summer for US southern and western urban areas during 1998-2013, which are opposite to the O_3 increases within the MMA.

The decreases in tropospheric O_3 in response to the abatement of emissions of O_3 precursors in US urban areas reported by Strode et al. (2015), are consistent with the trends within the MCMA observed here for NO_x and O_3, and with the decrease in the average concentrations of VOCs of around 2.4 ppb yr^{-1} since 2002, mostly propane, ethanol and acetone, reported by Garzón et al. (2016). Compared with other urban areas, the average increase in O_3 of 0.20 ppb yr^{-1} within the MMA is similar to those of 0.22-0.37 ppb yr^{-1} reported by Akimoto et al. (2015) in 4 urban areas of Japan during 1990-2010, and lower than that of ca. 0.5 ppb yr^{-1} reported by Bigi and Harrison (2010) in central London during 1996-2008, which were ascribed to faster decreases in NO_x than VOCs emissions. Finally, the results obtained here demonstrate the merits of the assessment and analysis of long-term continuous data for air quality and air pollutant emissions, with continued monitoring required to confirm the observed positive trend and growth rate of O_3 within the MMA and, to better understand the changes in regional and urban O_3.

3.8 Compliance with the 1-h and 8-h O_3 Mexican Standards

In Mexico, the running 8-h average standard of 80 ppb O_3 is considered to be breached if more than 4 exceedances occur in a calendar year, whereas the 1-h average standard sets a maximum permitted limit of 110 ppb O_3 (NOM-020-SSA1-1993). Since 19 Oct 2014, there have been new maximum permitted levels of a 1-h average of 95 ppb O_3 and a running 8-h average of 70 ppb O_3, respectively

(NOM-020-SSA1-2014). Such standards are applicable for whole calendar years and were not used in this study to determine the annual exceedances. Figure 14 shows that both standards are exceeded within the MMA, most frequently at STA followed by SNB, GPE and OBI, which has the largest growth rate of O_3, whereas the fewest breaches are observed at SNN. The number of exceedances decreased clearly during 1994-1995, 1999-2000, and sharply in 2009, at all sites, except for STA. This is in good agreement with decreases in the GDP, and also likely in O_3 precursor emissions, during the economic crisis and the national recession experienced in Mexico between 1994-1996 and 2000-2001, respectively (Fig. S8), and during the 2008-2009 global economic recession also observed over European (Castellanos and Boersma, 2012) and US urban regions (Russell et al., 2012).

Between 2012-2013, the number of annual exceedances decreased at all sites, possibly ascribed to an acute deacceleration of the Mexican economy reflected in declines in ground-level NO_x, which is observed particularly at SNN (Fig. 10). Such decrease in primary emissions from the industries upwind the urban area may impact positively the MMA airshed, leading to the observed decreases in annual exceedances. When the annual exceedances were tested for linear trends, SNN and SNB showed significant (p<0.05) growing trends of 0.23 and 0.50 exceedances yr^{-1} in the 1-h NOM, and for the 8-h running NOM, GPE, SNN SNB showed significant (p<0.1) growing trends of 1.73, 1.70 and 3.09 exceedances yr^{-1}, respectively. If the trends are tested for annual exceedances after 2000, the only significant change is a decrease in the growth rate at SNB to 1.83 exceedances yr^{-1} (p<0.1). This suggests that according to the long-term trends in O_3 and NO_x calculated within the MMA, the number of annual exceedances of the O_3 NOM standards will likely increase in response to increases in precursor emissions. Finally, based on the results reported here, it is recommended that more stringent emission controls are introduced, particularly for industries located upwind the MMA in order to improve air quality within the whole urban area.

4. Conclusions

The impact of changes in NO_x and VOCs emissions over O_3 long-term trends in the MMA, MCMA and GMA has been addressed by the first time in this study. Continuous high-frequency and high-precision O_3 data recorded during 1993-2014 at 5 sites within the MMA and 29 sites within the MCMA, and during 1996-2014 at 10 sites within the GMA, were used to calculate long-term trends. Within the MMA, the greatest mixing ratios of O_3 were recorded at downwind sites in E and SE air masses, representing the transport of precursors from industrial sources, dominant in the periphery of the MMA. The lowest O_3 mixing ratios were recorded at SNN, and for all sites were observed for the W and SW sectors, where air masses travel from central Mexico over 100-300 km of semi-arid region sparsely populated. Maximum daily 1-h values of O_3 and O_x increased significantly at GPE, SNN and SNB, owing to increasing emissions of precursors, while at OBI increasing O_3 and decreasing O_x trends arise from the local decrease of NO_x emissions from automobiles.

The O_3 seasonal cycles are driven mostly by temporal variations of meteorology. The largest and lowest AV_d are observed in summer and winter, respectively, for all sites, while the largest values correspond to STA result of stagnant air masses. Annual cycles at all sites peak in spring and through in winter, respectively, with a downward spike during summer caused by high winds that disperse O_3, and increase the boundary layer height. Decreases in O_3 precursor emissions during the economic crisis experienced in the country between 1994-1996, caused significant decline trends in AV_s from 1993 to 1997 or 1998, depending on site, followed by increasing trends in AV_s derived of the recovery of the economy, which is underlined by the greatest increase of AV_s observed at the industrial site SNN.

At all metropolitan areas, O_3 peaks after mid-day and dips before sunrise, though the peak value for the MCMA occurs around an hour earlier than for the MMA and GMA caused by the accelerated photo-chemical production of O_3 during late morning. Larger AV_d are seen at MCMA than at GMA and MMA related to the relative emissions of the O_3 precursors. Non-significant differences at any of the metropolitan areas between O_3 AV_d during weekends and weekdays are observed. This lack of the weekend effect is likely due to weekday O_3 production being limited by VOCs and inhibited by NO_x; whereas increases in the VOC/NO_x ratio during weekends in response to reduced emissions from mobile sources results in similar O_3 mixing ratios that during weekdays.

The largest O_3 growth rates were observed in the upper data distribution, and in sites near the industrial area located east of the MMA. Significant increasing linear trends in NO_x were observed at all sites, except at OBI, confirming the dominant role of increasing precursor emissions on the observed O_3 trends. A significant increasing trend of 0.20 ppb O_3 yr^{-1} within the MMA contrasts within a significant decreasing trend of -0.71 ppb O_3 yr^{-1} within the MCMA during 1993-2014, whereas a non-significant trend is evident within the GMA during 1996-2014. At the MCMA and MMA, the observed O_3 trends reflect the changes in tropospheric precursor levels. According to the long-term trends in O_3 for the MMA, the number of exceedances of the air quality standards will very likely increase as result of increasing precursor emissions. This emphasises the need for more stringent control of emissions in order to improve air quality within the MMA.

5. Acknowledgments

This research was supported by Tecnologico de Monterrey through the Research Group for Energy and Climate Change (Grant 0824A0104 and 002EICIR01). Grateful acknowledgements are made to the Secretariat for Sustainable Development of the Nuevo Leon State, the Secretariat for the Environment of Mexico City and the Secretariat for the Environment and Territorial Development of the Jalisco State for the public domain records. We gratefully thank the NOAA Air Resources Laboratory (ARL) for provision of the HYSPLIT model and READY website (http://www.ready.noaa.gov). The authors acknowledge Dr. Sigfrido Iglesias for providing imputed O_3 and NO_x data for the MMA time-series. We

are also grateful to Professor Paul Monks and Professor Richard Derwent for encouraging comments on an earlier version of the manuscript.

6. References

Akimoto, H., Mori, Y., Sasaki, K., Nakanishi, H., Ohizumi, T., and Itano, Y.: Analysis of monitoring data of ground-level ozone in Japan for long-term trend during 1990-2010: Causes of temporal and spatial variation, Atmos. Environ., 102, 302-310, doi:10.1016/j.atmosenv.2014.12.001, 2015.

Atkinson, R.: Atmospheric chemistry of VOCs and NOx. Atmos. Environ., 34, 2063-2101, doi:10.1016/S1352-2310(99)00460-4, 2000.

Benítez-García, S. E., Kanda, I., Wakamatsu, S., Okazaki, Y., and Kawano, M.: Analysis of criteria air pollutant trends in three Mexican metropolitan areas, Atmosphere, 5, 806-829, doi:10.3390/atmos5040806, 2014.

Bigi, A., and Harrison, R. M.: Analysis of the air pollution climate at a central urban background site, Atmos. Environ., 44, 2004-2012, doi:10.1016/j.atmosenv.2010.02.028, 2010.

Boersma, K. F., Jacob, D. J., Bucsela, E. J., Perring, A. E., Dirksen, R., van der A, R. J., Yantosca, R. M., Park, R. J., Wenig, M. O., Bertram, T. H., and Cohen, R. C.: Validation of OMI tropospheric NO2 observations during INTEX-B and application to constrain NOx emissions over the eastern United States and Mexico, Atmos. Environ., 42, 4480-4497. doi:10.1016/j.atmosenv.2008.02.004, 2008.

Butler, T. M., Stock, Z. S., Russo, M. R., Denier Van Der Gon, H. A. C., and Lawrence, M. G.: Megacity ozone air quality under four alternative future scenarios, Atmos. Chem. Phys., 12, 4413-4428, doi:10.5194/acp-12-4413-2012, 2012

Camalier, L., Cox, W., and Dolwick, P.: The effects of meteorology onozone in urban areas and their use in assessing ozone trends, Atmos. Environ., 41, 7127-7137, doi: 10.1016/j.atmosenv.2007.04.061, 2007.

Carslaw, D. C., and Ropkins, K.: openair - An R package for air quality data analysis, Environ. Model. Soft., 27-28, 52-61, doi:10.1016/j.envsoft.2011.09.008, 2012.

Carslaw, D. C.: The openair manual - open-source tools for analysing air pollution data, Manual for version 1.1-4, King's College London, 2015.

Castellanos, P. and Boersma, K. F.: Reductions in nitrogen oxides over Europe driven by environmental policy and economic recession, Sci. Rep., 2, doi:10.1038/srep00265, 2012.

Cleveland, R. B., Cleveland, W. S., McRae, J., and Terpenning, I.: STL: A seasonal-trend decomposition procedure based on Loess, J. Off. Stats., 6, 3-33, 1990.

Dentener, F., Stevenson, D., Cofala, J., Mechler, R., Amann, M., Bergamaschi, P., Raes, F., and Derwent, R.: The impact of air pollutant and methane emission controls on tropospheric ozone and radiative forcing: CTM calculations for the period 1990-2030, Atmos. Chem. Phys., 5, 1731-1755, doi:10.5194/acp-5-1731-2005, 2005.

Duncan, B. N., Lamsal, L. N., Thompson, A. M., Yoshida, Y., Lu, Z., Streets, D. G., Hurwitz, M. M., and Pickering, K. E.: A space-based, high-resolution view of notable changes in urban NOx pollution around the world (2005–2014), J. Geophys. Res., 121, 976–996, doi:10.1002/2015JD024121, 2016.

Durbin, J., and Koopman, S. J.: Time Series Analysis by State Space Methods, Oxford University Press, Oxford UK, 2nd Edition, 2012.

EPA (Environmental Protection Agency US): Compilation of Air Pollution Emission Factors (AP-42), Volume I: Stationary Point and Area Sources, available at: https://www.epa.gov/air-emissions-factors-and-quantification/ap-42-compilation-air-emission-factors, last access: 14 Jan 2017, 1995.

EPA (Environmental Protection Agency US): User's Guide to MOBILE6.1 and MOBILE6.2: Mobile Source Emission Factor Model, available at: https://www3.epa.gov/otaq/models/mobile6/420r03010.pdf, last access: 16 Jan 2017, 2003.

EPA (Environmental Protection Agency US): Air quality trends, available at: https://www.epa.gov/air-trends, last access: 15 Jan 2017, 2009.

Escamilla-Nuñez, M. -C., Barraza-Villarreal, A., Hernandez-Cadena, L., Moreno-Macias, H., Ramirez-Aguilar, M., Sienra-Monge, J. -J., Cortez-Lugo, M., Texcalac, J.-L., del Rio-Navarro, B., and Romieu, I.: Traffic-related air pollution and respiratory symptoms among asthmatic children, resident in Mexico City: The EVA cohort study, Respir. Res., 9, doi:10.1186/1465-9921-9-74, 2008.

Garzón, J. P., Huertas, J. I., Magaña, M., Huertas, M. E., Cárdenas, B., Watanabe, T., Maeda, T., Wakamatsu, S., and Blanco, S.: Volatile organic compounds in the atmosphere of Mexico City, Atmos. Environ., 119, 415-429, doi:10.1016/j.atmosenv.2015.08.014, 2015.

Guicherit, R., and Roemer, M.: Tropospheric ozone trends, Chemosphere, 2, 167-183, doi:10.1016/S1465-9972(00)00008-8, 2000.

Hernández-Paniagua, I. Y., Lowry, D., Clemitshaw, K. C., Fisher, R. E., France, J. L., Lanoisellé, M., Ramonet, M., and Nisbet, E. G.: Diurnal, seasonal, and annual trends in atmospheric CO2 at southwest London during 2000-2012: Wind sector analysis and comparison with Mace Head, Ireland, Atmos. Environ., 105, 138-147, doi: 10.1016/j.atmosenv.2015.01.02, 2015.

INE (Instituto Nacional de Ecologia): Cuarto almanaque de datos y tendencias de la calidad del aire en 20 ciudades mexicanas 2000-2009, INE-SEMARNAT, México, D.F., 405 pp., 2011.

INEGI (National Institute of Statistics and Geography): XIII Censo General de

Población y Vivienda 2010, México, available at: http://www.censo2010.org.mx/, last Access: 22 May 2016, 2010.

INEGI (National Institute of Statistics and Geography): México en Cifras, México, available at: http://www3.inegi.org.mx/sistemas/mexicocifras/default.aspx?e=19, last access: 22 May 2016, 2015.

INEGI (National Institute of Statistics and Geography): Producto Interno Bruto (GDP)–Trimestral 2016, available at: http://www.inegi.org.mx/est/contenidos/proyectos/cn/pibt/, last access: 11 Jan 2017, 2016.

IPCC: Climate Change 2013: The Physical Science Basis. Contribution of Working Group I to the Fifth Assessment Report of the Intergovernmental Panel on Climate Change, 2013. [Stocker, T.F., D. Qin, G.-K. Plattner, M. Tignor, S.K. Allen, J. Boschung, A. Nauels, Y. Xia, V. Bex and P.M. Midgley (eds.)]. Cambridge University Press, Cambridge, United Kingdom and New York, NY, USA, 1535 pp., 2013.

Jaimes, P. M., Bravo, A. H., Sosa, E. R., Cureño, G. I., Retama, H. A., Granados, G. G., and Becerra, A. E.: Surface ozone concentration trends in Mexico City Metropolitan Area, in: Proceedings of the Air and Waste Management Association's Annual Conference and Exhibition AWMA, San Antonio, Texas, 19-22 June 2012, 3, 2273-2284, 2012.

Jaimes-Palomera, M., Retama, A., Elias-Castro, G., Neria-Hernández, A., Rivera-Hernández, O., and Velasco, E.: Non-methane hydrocarbons in the atmosphere of Mexico City: Results of the 2012 ozone-season campaign, Atmos. Environ., 132, 258-275, doi:10.1016/j.atmosenv.2016.02.047, 2016.

Jenkin, M. E., and Clemitshaw, K. C.: Ozone and other secondary photochemical pollutants: chemical processes governing their formation in the planetary boundary layer, Atmos. Environ., 34(16), 2499-2527, doi:10.1016/S1352-2310(99)00478-1, 2000.

Kumar, A., Wu, S., Weise, M. F., Honrath, R., Owen, R. C., Helmig, D., Kramer, L., Val Martin, M., and Li, Q.: Free-troposphere ozone and carbon monoxide over the North Atlantic for 2001-2011, Atmos. Chem. Phys., 13, 12537-12547, doi:10.5194/acp-13-12537-2013, 2013.

769 Lee, Y. C., Shindell, D. T., Faluvegi, G., Wenig, M., Lam, Y. F., Ning, Z., Hao, S., and Lai, C. S.: Increase
770 of ozone concentrations, its temperature sensitivity and the precursor factor in South China, Tellus B.
771 Chem. Phys. Meteorol., 66, doi:10.3402/tellusb.v66.23455, 2014.

772 Lefohn, A. S., Shadwick, D., and Oltmans, S. J.: Characterizing changes in surface ozone levels in
773 metropolitan and rural areas in the United States for 1980−2008 and 1994−2008, Atmos. Environ, 44,
774 5199−5210, doi: 10.1016/j.atmosenv.2010.08.049, 2010.

775 Lei, W., de Foy, B., Zavala, M., Volkamer, R., and Molina, L. T.: Characterizing ozone production in the
776 Mexico City Metropolitan Area: a case study using a chemical transport model, Atmos. Chem. Phys., 7,
777 1347-1366, doi:10.5194/acp-7-1347-2007, 2007.

778 Lelieveld, J., and Dentener, F. J.: What controls tropospheric ozone?, J. Geophys. Res., 105(D3), 3531-
779 3551, doi:10.1029/1999JD901011, 2000.

780 Lelieveld, J., Evans, J. S., Fnais, M., Giannadaki, D., and Pozzer, A.: The contribution of outdoor air
781 pollution sources to premature mortality on a global scale, Nature Letts., 15371,
782 doi:10.1038/nature15371, 2015.

783 Menchaca-Torre, H. L., Mercado-Hernández, R., and Mendoza-Domínguez, A.: Diurnal and seasonal
784 variation of volatile organic compounds in the atmosphere of Monterrey, Mexico, Atmos. Poll. Res., 6,
785 1073-1081, doi:10.1016/j.apr.2015.06.004, 2015.

786 Molina, M. J., and Molina, L. T.: Megacities and atmospheric pollution, J. Air Waste Manage., 54, 644-
787 680, doi:10.1080/10473289.2004.10470936, 2004.

788 Monks, P. S.: A review of the observations and origins of the spring ozone maximum, Atmos. Environ.,
789 34, 3545-3561, doi:10.1016/S1352-2310(00)00129-1, 2000.

790 Monks, P. S., Archibald, A. T., Colette, A., Cooper, O., Coyle, M., Derwent, R., Fowler, D., Granier, C.,
791 Law, K. S., Mills, G. E., Stevenson, D. S., Tarasova, O., Thouret, V., von Schneidemesser, E.,
792 Sommariva, R., Wild, O., and Williams, M. L.: Tropospheric ozone and its precursors from the urban to
793 the global scale from air quality to short-lived climate forcer, Atmos. Chem. Phys., 15, 8889-8973,
794 doi:10.5194/acp-15-8889-2015, 2015.

795 Parrish, D. D., Singh, H. B., Molina, L., and Madronich, S.: Air quality progress in North American
796 megacities: A review, Atmos. Environ., 45, 7015-7025, doi:10.1016/j.atmosenv.2011.09.039, 2011.

797 ProAire-AMM (Programa de Gestión para Mejorar la Calidad del Aire del Área Metropolitana de
798 Monterrey 2008-2012), SEMARNAT, Gobierno del estado de Nuevo León, available at:
799 http://www.semarnat.gob.mx/archivosanteriores/temas/gestionambiental/calidaddelaire/
800 Documents/Calidad%20del%20aire/Proaires/ProAires_Vigentes/6_ProAire%20AMM%202008-
801 2012.pdf, last access: 22 May 2016, 2008.

802 Pugliese, S. C., Murphy, J. G., Geddes, J. A., and Wang, J. M.: The impacts of precursor reduction and
803 meteorology on ground-level ozone in the Greater Toronto Area, Atmos. Chem. Phys., 14, 8197-8207,
804 doi:10.5194/acp-14-8197-2014, 2014.

805 Pusede, S. E., Gentner, D. R., Wooldridge, P. J., Browne, E. C., Rollins, A. W., Min, K.-E., Russell, A.
806 R., Thomas, J., Zhang, L., Brune, W. H., Henry, S. B., DiGangi, J. P., Keutsch, F. N., Harrold, S. A.,
807 Thornton, J. A., Beaver, M. R., St. Clair, J. M., Wennberg, P. O., Sanders, J., Ren, X., VandenBoer, T.
808 C., Markovic, M. Z., Guha, A., Weber, R., Goldstein, A. H., and Cohen, R. C.: On the temperature
809 dependence of organic reactivity, nitrogen oxides, ozone production, and the impact of emission controls
810 in San Joaquin Valley, California, Atmos. Chem. Phys., 14, 3373-3395, doi:10.5194/acp-14-3373-2014,
811 2014.

812 Pusede, S. E., Steiner, A. L., and Cohen, R.C.: Temperature and Recent Trends in the Chemistry of
813 Continental Surface Ozone, Chem. Rev., 115, 3898-3918, doi: 10.1021/cr5006815, 2015.

814 R Core Team: R: a Language and Environment for Statistical Computing, R

Foundation for Statistical Computing, Vienna, Austria, ISBN 3-900051-07-0, 2013, available at: www.R-project.org, last access: 23 May 2016, 2013.

Radian (International): MEXICO EMISSIONS INVENTORY PROGRAM MANUALS (Vol. II-VI), available at: https://www3.epa.gov/ttncatc1/cica/other3_s.html, last access: 15 Jan 2017, 2000.

Reinsel, G. C.: Elements of Multivariate Time Series Analysis. Springer-Verlag, New York, USA, 2nd Edition, 1997.

Revell, L. E., Tummon, F., Stenke, A., Sukhodolov, T., Coulon, A., Rozanov, E., Garny, H., Grewe, V. and Peter, T.: Drivers of the tropospheric ozone budget throughout the 21st century under the medium-high climate scenario RCP 6.0, Atmos. Chem. Phys., 15, 5887-5902, doi:10.5194/acp-15-5887-2015, 2015.

Rodríguez, S., Huerta, G., and Reyes, H.: A study of trends for Mexico City ozone extremes: 2001-2014, Atmosfera, 29, 107-120, doi:http://dx.doi.org/10.20937/ATM.2016.29.02.01, 2016.

Russell, A. R., Valin, L. C., and Cohen, R. C.: Trends in OMI NO2 observations over the United States: effects of emission control technology and the economic recession, Atmos. Chem. Phys., 12, 12197-12209, doi:10.5194/acp-12-12197-2012, 2012.

Salmi, T., Määttä, A., Anttila, P., Ruoho-Airola, T. and Amnell, T.: Detecting trends of annual values of atmospheric pollutants by the Mann-Kendall test and Sen's slope estimates – the Excel template application MAKESENS, Publications on Air Quality Report code FMI-AQ-31, Helsinki, Finland, 31, 1-35, 2002.

Sather, M.E. and Cavender, K.: Trends analyses of 30 years of ambient 8 hour ozone and precursor monitoring data in the South Central US: progress and challenges, Environ. Sci. Proc. Imp., 18, 819-831. 2016.

Schultz, M., and Rast, S.: REanalysos of the TROpospheric chemical composition over the past 40 years, Emission Data Sets and Methodologies for Estimating Emissions, Work Package 1, Deliverable D1-6, available at: http://retro-archive.iek.fz-juelich.de/data/documents/reports/D1-6_final.pdf, last access: 14 Jul 2016, 2007.

SDS (Secretaria de Desarrollo Sustentable), Inventario de emisiones del Área Metropolitana de Monterrey 2013, personal communication, Monterrey, N.L. México, 4 Sep 2015.

SDS (Secretaria de Desarrollo Sustentable): Sistema Integral de Monitoreo Ambiental, available at: http://aire.nl.gob.mx/, last access: 21 May 2016, 2016.

SEDEMA (Secretaria del Medio Ambiente): INVENTARIO de Emisiones a la Atmosfera en la ZMVM 1996, available at: http://www.sedema.df.gob.mx/flippingbook/inventario-emisiones-1996/#p=1, last access: 20 May 2016, 1999.

SEDEMA (Secretaria del Medio Ambiente): Inventario de Emisiones Zona Metropolitana del Valle de Mexico 1998, available at: http://www.sedema.df.gob.mx/flippingbook/inventario-emisiones-zmvm1998/#p=75, last access: 20 May 2016, 2001.

SEDEMA (Secretaria del Medio Ambiente): Inventario de emisiones a la Atmosfera Zona Metropolitana del Valle de Mexico 2000, available at: http://www.sedema.df.gob.mx/ flippingbook/inventario-emisiones-zmvm2000/, last access: 20 May 2016, 2003.

SEDEMA (Secretaria del Medio Ambiente): Inventario de emisiones de la Zona Metropolitana del Valle de Mexico 2002, available at: http://www.sedema.df.gob.mx/flippingbook/inventario-emisiones-zmvm-criterio2004/#p=1, last access: 20 May 2016, 2004.

SEDEMA (Secretaria del Medio Ambiente): Inventario de Emisiones Zona Metropolitana del Valle de Mexico 2004, available at: http://www.sedema.df.gob.mx/flippingbook/inventario-emisiones-zmvm-criterio2004/#p=1, last access: 20 May 2016, 2006.

SEDEMA (Secretaria del Medio Ambiente): Inventario de Emisiones de CONTAMINANTES CRITERIO 2006, available at: http://www.sedema.df.gob.mx/flippingbook/inventario-emisiones-zmvm-criterio2006/#p=1, last access: 20 May 2016, 2008.

SEDEMA (Secretaria del Medio Ambiente): Inventario de emisiones de contaminantes criterio de la ZMVM 2008, available at: http://www.sedema.df.gob.mx/flippingbook/inventario-emisiones-zmvm-criterio2008/#p=1, last access: 20 May 2016, 2010.

SEDEMA (Secretaria del Medio Ambiente): INVENTARIO DE EMISIONES DE LA ZONA METROPOLITANA DEL VALLE DE MEXICO CONTAMINANTES CRITERIO 2010, available at: http://www.sedema.df.gob.mx/flippingbook/inventario-em1isiones-zmvm-criterio-2010/#p=6, last access: 20 May 2016, 2012.

SEDEMA (Secretaria del Medio Ambiente): Inventario de emisiones contaminantes y de efecto invernadero, available at: http://www.sedema.df.gob.mx/flippingbook/inventario-emisioneszmvm2012/, last access: 20 May 2016, 2014.

SEDEMA (Secretaria del Medio Ambiente de la Ciudad de Mexico): Sistema de Monitoreo Atmosférico, available at: http://www.aire.df.gob.mx/default.php, last access: 21 May 2016, 2016a.

SEDEMA (Secretaria del Medio Ambiente de la Ciudad de Mexico): Inventario de Emisiones de la CDMX 2014 Contaminantes Criterio Tóxicos y de Efecto Invernadero, available at: http://www.aire.cdmx.gob.mx/descargas/publicaciones/flippingbook/inventario-emisiones-cdmx2014-2/, last Access: 10 Jan 2017, 2016b.

SEMARNAT (Secretaria del Medio Ambiente y Recursos Naturales): Inventario Nacional de Emisiones 1999, México, D.F., available at: http://www.inecc.gob.mx/dica/548-calaire-inem-1999, last access: 20 May 2016, 2006.

SEMARNAT (Secretaria del Medio Ambiente y Recursos Naturales): Inventario Nacional de Emisiones 2005, México, D.F., available at: http://sinea.semarnat.gob.mx/sinae.php?process= UkVQT1JURUFET1I=&categ=1, last access: 22 May 2016, 2011.

SEMARNAT (Secretaria del Medio Ambiente y Recursos Naturales): Inventario Nacional de Emisiones 2008, México, D.F., available at: http://sinea.semarnat.gob.mx/ sinae.php?process= UkVQT1JURUFET1I=&categ=14, last access: 22 May 2016, 2014.

SEMARNAT (Secretaria del Medio Ambiente y Recursos Naturales): Informe Nacional de calidad del aire 2014, México, D.F., available at: http://inecc.gob.mx/descargas/calaire/ 2015_Informe_nacional_calidad_aire_2014_Final.pdf, last access: 15 Dec 2016, 2015.

SENER (Secretaria de Energia): Estadísticas Energéticas Nacionales, México, available at: http://sie.energia.gob.mx/bdiController.do?action=temas, last access: 4 November 2015, 2015.

Sicard, P., Serra, R., and Rossello, P.: Spatiotemporal trends in ground-level ozone concentrations and metrics in France over the time period 1999-2012, Environ. Res., 149, 122-144, doi:10.1016/j.envres.2016.05.014, 2016

Sierra, A., Vanoye, A. Y., and Mendoza, A.: Ozone sensitivity to its precursor emissions in northeastern Mexico for a summer air pollution episode, J. Air Waste Manage., 63, 1221-1233, doi:10.1080/10962247.2013.813875, 2013.

Simon, H., Reff, A., Wells, B., Xing, J., and Frank, N.: Ozone trends across the United States over a period of decreasing NOx and VOC emissions, Environ. Sci. Tech., 49, 186-195. doi:10.1021/es504514z, 2015.

SMN (Servicio Meteorológico Nacional), available at: http://smn.cna.gob.mx/es/, last access: 21 May 2016.

Song, J., Lei, W., Bei, N., Zavala, M., de Foy, B., Volkamer, R., Cardenas, B., Zheng, J., Zhang, R., and Molina, L. T.: Ozone response to emission changes: a modeling study during the MCMA-2006/MILAGRO Campaign, Atmos. Chem. Phys., 10, 3827-3846, doi:10.5194/acp-10-3827-2010, 2010.

Staehelin, J., and Schmid, W.: Trend analysis of tropospheric ozone concentrations utilizing the 20-year data set of ozone balloon soundings over Payerne (Switzerland), Atmos. Environ., 25, 1739-1749, doi:10.1016/0960-1686(91)90258-9, 1991.

Stein, A. F., Draxler, R. R., Rolph, G. D., Stunder, B. J. B., Cohen, M. D., and Ngan, F.: NOAA'S HYSPLIT ATMOSPHERIC TRANSPORT AND DISPERSION MODELING SYSTEM, Bull. Am. Meteorol. Soc., 96, 2059-2077, doi:10.1175/BAMS-D-14-00110.1, 2015.

Steiner, A. L., Davis, A. J., Sillman, S., Owen, R. C., Michalak, A. M., and Fiore, A. M: Observed suppression of ozone formation at extremely high temperatures due to chemical and biophysical feedbacks, Proc. Natl. Acad. Sci. U.S.A., 107, 19685-19690, doi:10.1073/pnas.1008336107, 2010.

Stephens, S., Madronich, S., Wu, F., Olson, J. B., Ramos, R., Retama, A., and Muñoz, R.: Weekly patterns of México City's surface concentrations of CO, NOx, PM10 and O3 during 1986-2007, Atmos. Chem. Phys., 8, 5313-5325, doi:10.5194/acp-8-5313-2008, 2008.

Stevenson, D. S., Dentener, F. J., Schultz, M. G., Ellingsen, K., van Noije, T. P. C., Wild, O., Zeng, G., Amann, M., Atherton, C. S., Bell, N., Bergmann, D. J., Bey, I., Butler, T., Cofala, J., Collins, W. J., Derwent, R. G., Doherty, R. M., Drevet, J., Eskes, H. J., Fiore, A. M., Gauss, M., Hauglustaine, D. A., Horowitz, L. W., Isaksen, I. S .A., Krol, M. C., Lamarque, J.-., Lawrence, M. G., Montanaro, V., Müller, J.-., Pitari, G., Prather, M. J., Pyle, J. A., Rast, S., Rodriguez, J. M., Sanderson, M. G., Savage, N. H., Shindell, D. T., Strahan, S. E., Sudo, K., and Szopa, S.: Multimodel ensemble simulations of present-day and near-future tropospheric ozone. J. Geophys. Res., D08301, doi: 10.1029/2005JD006338, 2006.

Strode, S. A., Rodriguez, J. M., Logan, J. A., Cooper, O. R., Witte, J. C., Lamsal, L. N., Damon, M., Van Aartsen, B., Steenrod, S. D., and Strahan, S. E.: Trends and variability in surface ozone over the United States, J. Geophys. Res., 120, 9020-9042, doi:10.1002/2014JD022784, 2015.

Tiwari, A. K., Suresh, K. G., Arouri, M., and Teulon, F.: Causality between consumer price and producer price: Evidence from Mexico. Economic Modelling, 36, 432-440, doi:10.1016/j.econmod.2013.09.050, 2014.

Torres-Jardón, R.: Comparative assessment of the sensitivity of ozone to nitrogen oxides and volatile organic compounds in two dissimilar metropolitan areas of North America: Cincinnati, OH (USA) and México City, D.F. (México). Ph. D. Dissertation, University of Cincinnati, 2004.

VanCuren, R.: Transport aloft drives peak ozone in the Mojave Desert, Atmos. Environ., 109, 331-341, doi: 10.1016/j.atmosenv.2014.09.057, 2015.

Vingarzan, R.: A review of surface ozone background levels and trends, Atmos. Environ., 38, 3431-3442, doi:10.1016/j.atmosenv.2004.03.030, 2004.

Velasco, E., Lamb, B., Westberg, H., Allwine, E., Sosa, G., Arriaga-Colina, J. L., Jobson, B. T., Alexander, M. L., Prazeller, P., Knighton, W. B., Rogers, T. M., Grutter, M., Herndon, S. C., Kolb, C. E., Zavala, M., de Foy, B., Volkamer, R., Molina, L. T., and Molina, M. J.: Distribution, magnitudes, reactivities, ratios and diurnal patterns of volatile organic compounds in the Valley of Mexico during the MCMA 2002 & 2003 field campaigns, Atmos. Chem. Phys., 7, 329-353, doi:10.5194/acp-7-329-2007, 2007.

Volkamer, R., Sheehy, P., Molina, L. T., and Molina, M. J.: Oxidative capacity of the Mexico City atmosphere-Part 1: A radical source perspective, Atmos. Chem. Phys., 10, 6969-6991, doi:10.5194/acp-10-6969-2010, 2010.

949 Wang, Y., Konopka, P., Liu, Y., Chen, H., Müller, R., Plöger, F., Riese, M., Cai, Z., and Lü, D.:
950 Tropospheric ozone trend over Beijing from 2002-2010: Ozonesonde measurements and modeling
951 analysis, Atmos. Chem. Phys., 12, 8389-8399, doi:10.5194/acp-12-8389-2012, 2012.

952 Wilson, R. C., Fleming, Z. L., Monks, P. S., Clain, G., Henne, S., Konovalov, I. B., Szopa, S., and Menut,
953 L.: Have primary emission reduction measures reduced ozone across Europe? An analysis of European
954 rural background ozone trends 1996-2005, Atmos. Chem. Phys., 12, 437-454, doi:10.5194/acp-12-437-
955 2012, 2012.

956 Wolff, G. T., Kahlbaum, D. F., and Heuss, J. M.: The vanishing ozone weekday/weekend effect, J. Air
957 Waste Manage., 63, 292-299, doi:10.1080/10962247.2012.749312, 2013.

958 World Health Organization: Ambient (outdoor) air quality and health, 2014 update,
959 http://www.who.int/mediacentre/factsheets/fs313/en/, last access: 21 May 2016.

960 Xing, J., Pleim, J., Mathur, R., Pouliot, G., Hogrefe, C., Gan, C.-M., and Wei, C.: Historical gaseous and
961 primary aerosol emissions in the United States from 1990 to 2010, Atmos. Chem. Phys., 13, 7531-7549,
962 doi:10.5194/acp-13-7531-2013, 2013.

963 Xu, X., Lin, W., Wang, T., Yan, P., Tang, J., Meng, Z., and Wang, Y.: Long-term trend of surface ozone
964 at a regional background station in eastern China 1991-2006: Enhanced variability, Atmos. Chem. Phys.,
965 8, 2595-2607, doi:10.5194/acp-8-2595-2008, 2008.

966 Zellweger, C., Hüglin, C., Klausen, J., Steinbacher, M., Vollmer, M., and Buchmann, B.: Inter-comparison
967 of four different carbon monoxide measurement techniques and evaluation of the long-term carbon
968 monoxide time series of Jungfraujoch, Atmos. Chem. Phys., 9, 3491-3503, doi:10.5194/acp-9-3491-
969 2009, 2009.

970 Zheng, J., Swall, J. L., Cox, W. M., and Davis, J. M. Interannual variation in meteorologically adjusted
971 ozone levels in the eastern United States: A comparison of two approaches, Atmos. Environ., 41, 705-
972 716, doi:10.1016/j.atmosenv.2006.09.010, 2007.

973

974 **Table 1.** Air quality limit values stated in the Mexican legislation.

Pollutant	Mexican Official Standard	Limit value*
O_3 (ppb)	NOM-020-SSA1-1993	110 (1-h), 80 (8-h)[a,b]
	NOM-020-SSA1-2014	95 (1-h) , 70 (8-h)[a,b]
PM_{10} ($\mu g\ m^{-3}$)	NOM-025-SSA1-1993	75 (24-h), 40 (1-yr)
	NOM-025-SSA1-2014	50 (24h), 35 (1-yr)
$PM_{2.5}$ ($\mu g\ m^{-3}$)	NOM-025-SSA1-1993	45 (24-h), 12 (1-yr)
	NOM-025-SSA1-2014	30 (24-h), 10 (1-yr)
CO (ppm)	NOM-02-SSA1-1993	11 (8-h)[b]
NO_2 (ppm)	NOM-023-SSA1 -1993	0.21 (1-h)

975 *Average period.
976 [a]Not to be exceeded more than 4 times in a calendar year.
977 [b]Running average.
978

Table 2. Site description, location and instrumentation used during 1993 to 2014 within the MMA.

Site	Code	Location	Elevation (m a.s.l.)	Site description
Guadalupe	GPE	25° 40.110' N, 100° 14.907' W	492	Urban background site in the La Pastora park, surrounded by a highly populated area, 450 m from Pablo Rivas Rd.
San Nicolas	SNN	25° 44.727' N, 100° 15.301' W	476	Urban site surrounded by a large number of industries and residential areas, 450 m from Juan Diego Diaz de Beriagna Rd.
Obispado	OBI	25° 40.561' N, 100° 20.314' W	560	Urban site near the city centre of MMA, 250 m from Jose Eleuterio González Rd. and 250 m from Antonio L. Rodríguez Rd.
San Bernabe	SNB	25° 45.415' N, 100° 21.949' W	571	Urban site in a residential area downwind of an industrial area with high traffic volume, 140 m from Aztlan Rd.
Santa Catarina	STA	25° 40.542' N, 100° 27.901' W	679	Urban site downwind of industrial sources, 200 m from Manuel Ordoñez Rd.

Table 3. Growth rates by wind sector in annual averages of O_3 in ppb yr^{-1} for 1993-2014 at the 5 sites within the MMA.

Site	N	NE	E	SE	S	SW	W	NW
GPE	0.23[c]	0.16[b]	0.43[c]	0.55[c]	0.23[c]	0.15[c]	0.05[a]	0.11[a]
SNN	0.16[c]	0.06	0.36[c]	0.46[c]	0.08	-0.05	0.04	0.03
OBI	0.08[b]	0.22[c]	0.50[c]	0.66[c]	0.32[c]	0.18[c]	0.06	0.06
SNB	0.36[c]	0.43[c]	0.43[c]	0.16[a]	-0.09	-0.06	-0.04	0.00
STA	0.00	0.02	0.06	0.25[c]	0.08[a]	0.00	-0.05[a]	-0.02

[a]Level of significance $p < 0.1$.
[b]Level of significance $p < 0.05$.
[c]Level of significance $p < 0.001$.

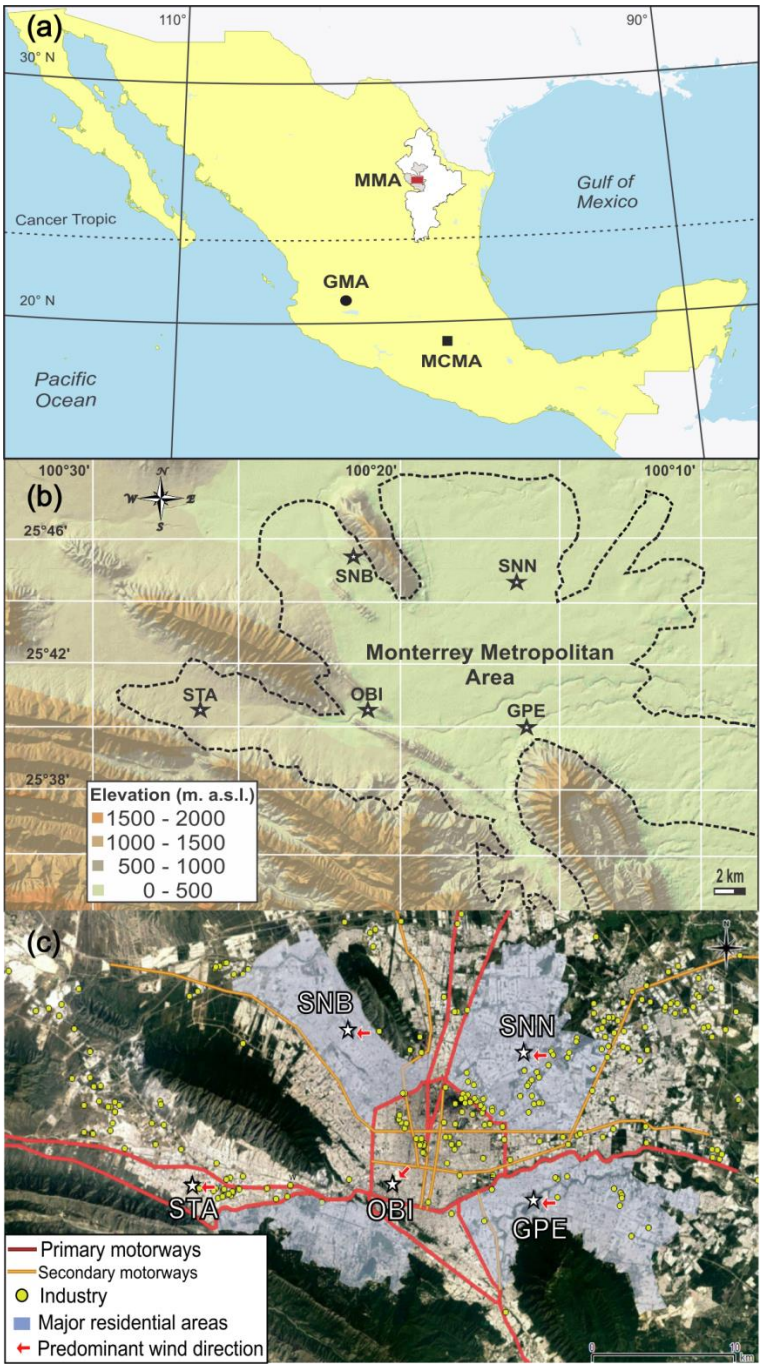

Fig. 1(a). The MMA, MCMA and GMA in the national context. **(b).** Topography of the MMA and distribution of the 5 monitoring sites over the area. **(c).** The 5 monitoring sites in relation to primary and secondary motorways, industries and major residential areas. The red arrows show the predominant wind direction at each site from 1993 to 2014.

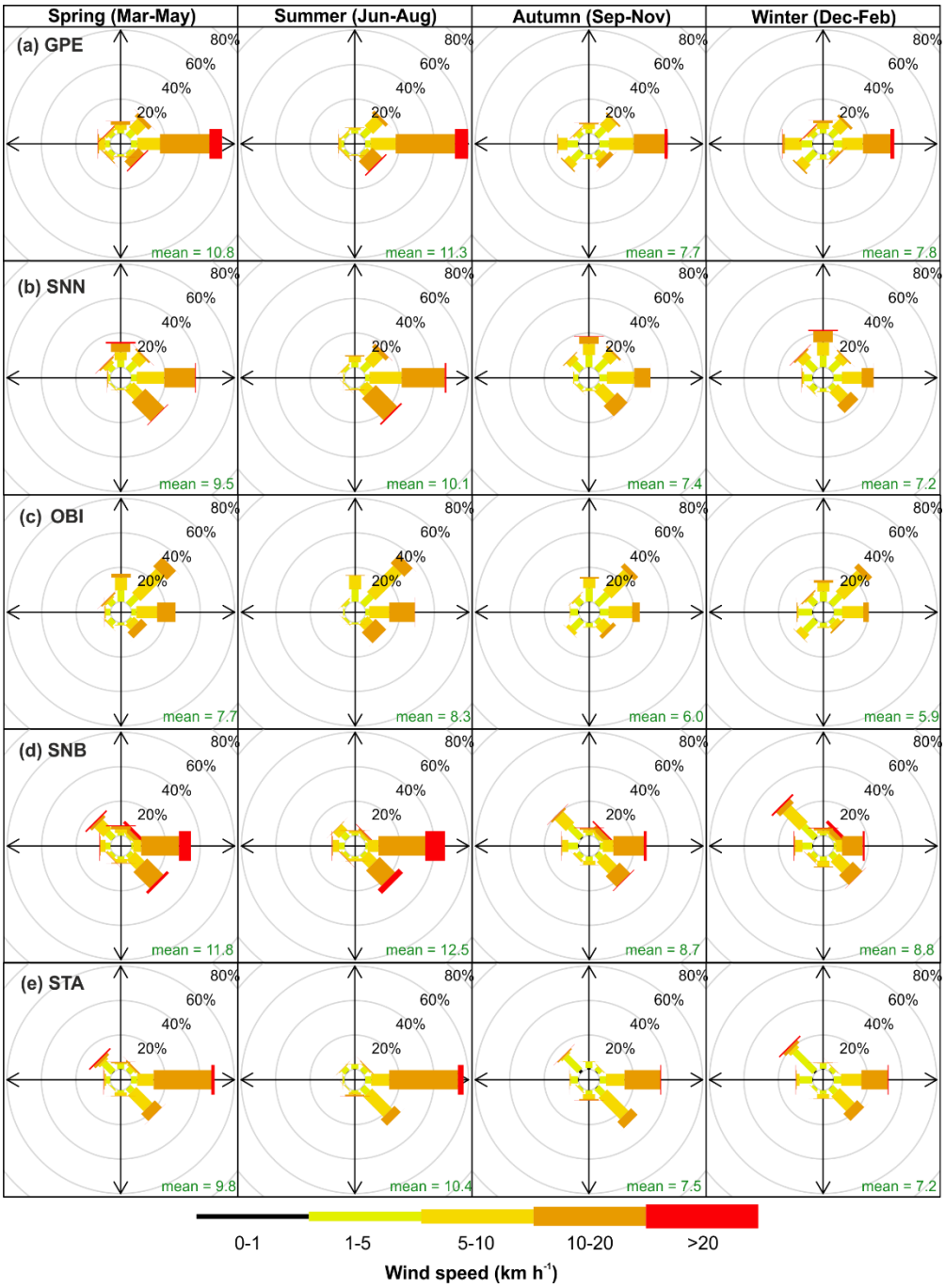

Fig. 2. Frequency of counts of measured wind direction occurrence by season and site within the MMA during 1993-2014.

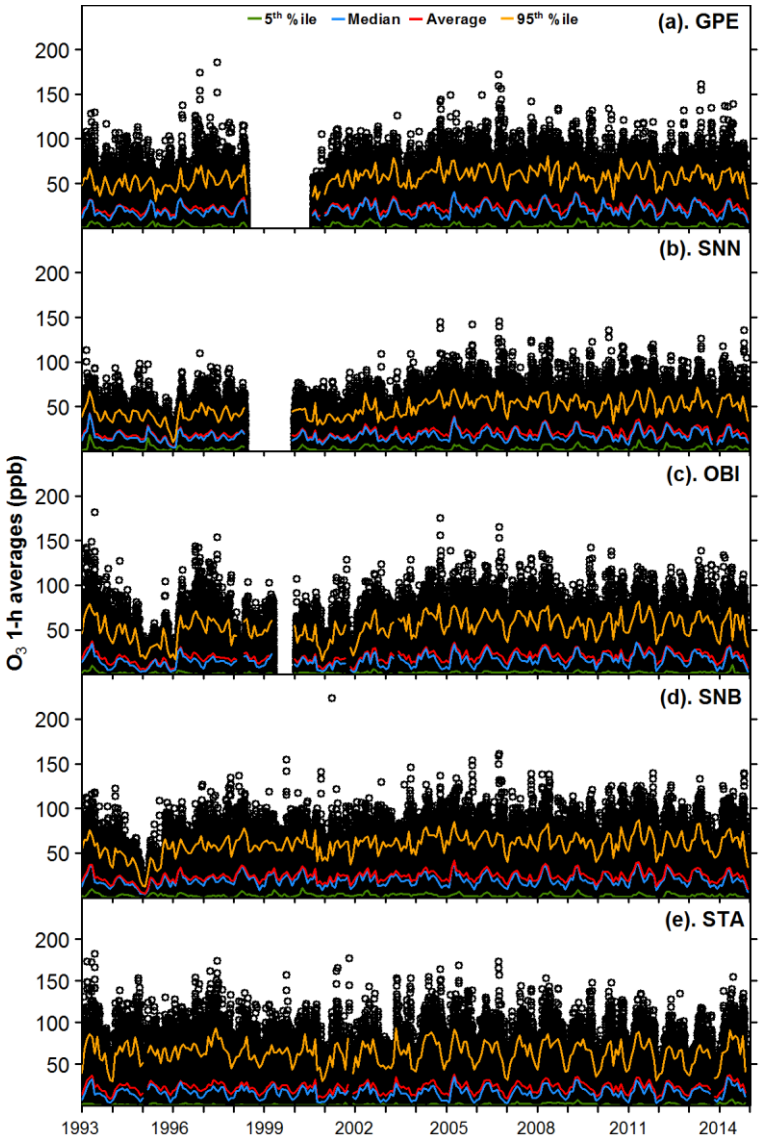

Fig. 3. 1-h averages of O_3 mixing ratios recorded from Jan 1993 to Dec 2014 within the MMA. The continuous lines show the monthly 5th (green) and 95th (orange) percentiles, medians (blue) and averages (red) of O_3 derived from daily data.

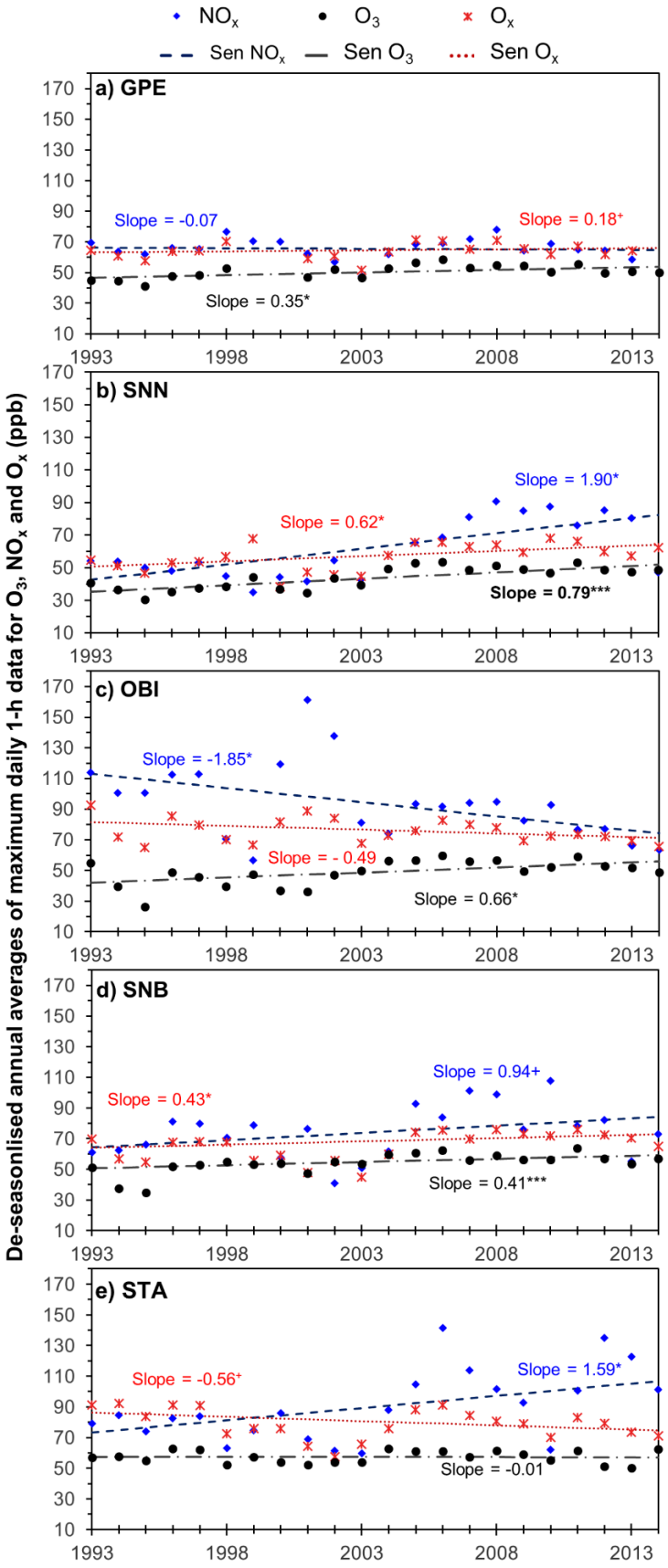

Fig. 4. Long-term trends of daily maximum 1-h values for NO_x, O_3 and O_x observed at the 5 monitoring sites during 1993- 2014 within the MMA. The slopes show annual rates of change expressed in units of ppb yr^{-1}. The dashed lines represent the Sen slopes. Statistical significance is expressed as $p<0.1$ =$^+$, $p<0.05$ = *, $p<0.01$ = ** and $p<0.001$ = ***.

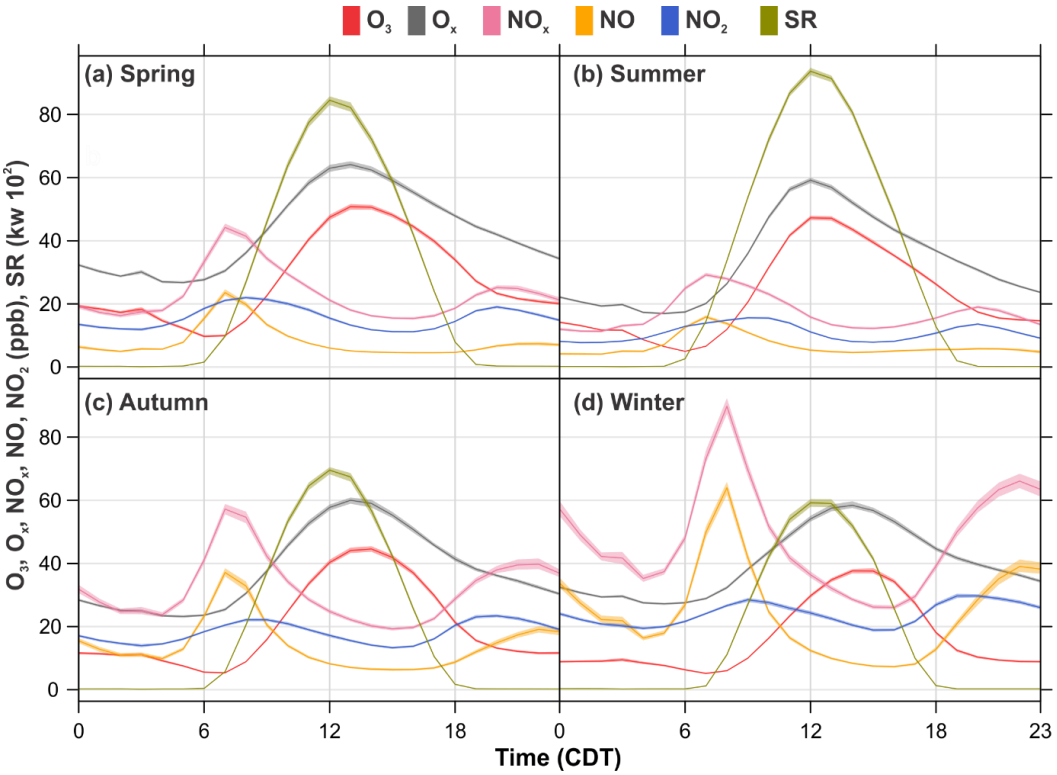

Fig. 5. Average daily profiles for O_3, O_x, NO_x, NO, NO_2 and SR within the MMA during 1993-2014. The shading shows the 95 % confidence intervals of the average.

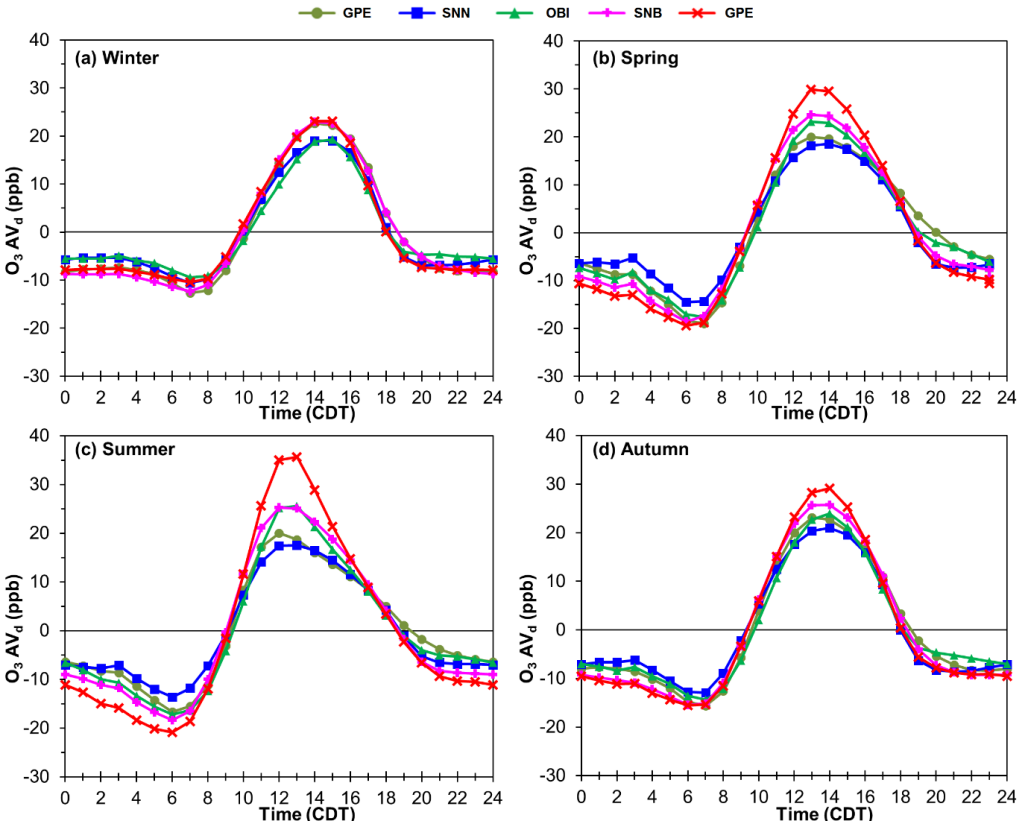

Fig. 6. O_3 de-trended daily profiles by season observed within the MMA during 1993-2014. De-trended O_3 daily cycles were constructed by subtracting daily averages from hourly averages to remove the impact of the long-term trends.

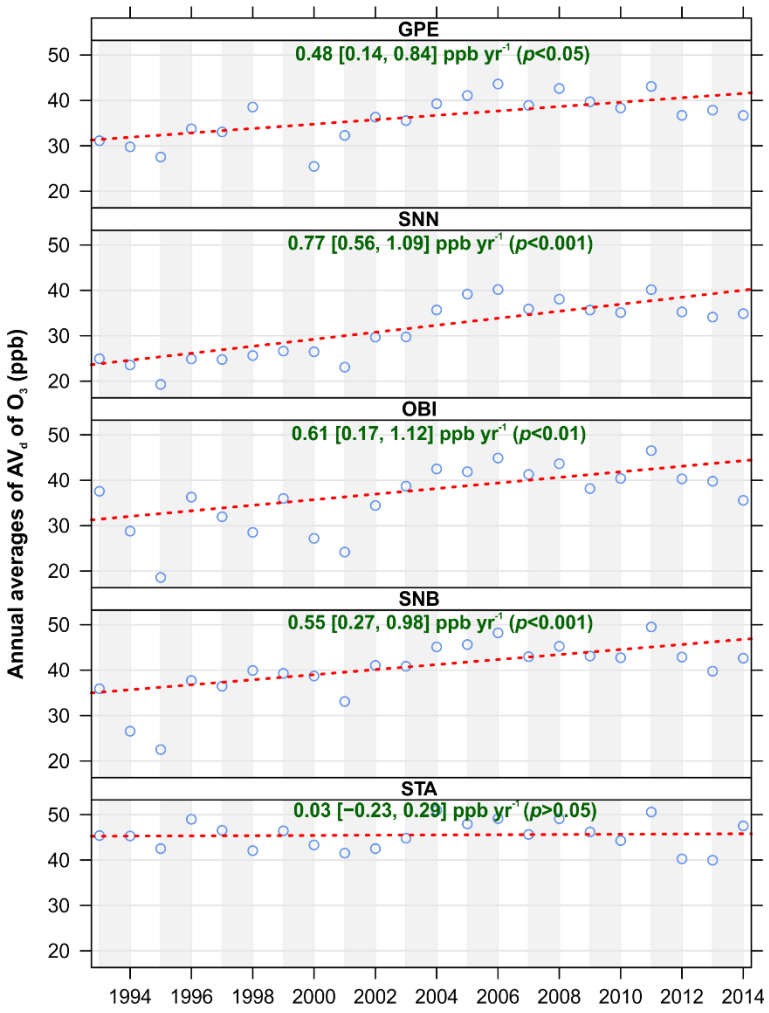

Fig. 7. Long-term trends of AV_d O_3 annual averages at the 5 sites within the MMA during 1993-2014. The dashed lines represent the Sen slopes. Statistical significance is expressed as $p<0.1$ =$^+$, $p<0.05$ = *, $p<0.01$ = ** and $p<0.001$ = ***.

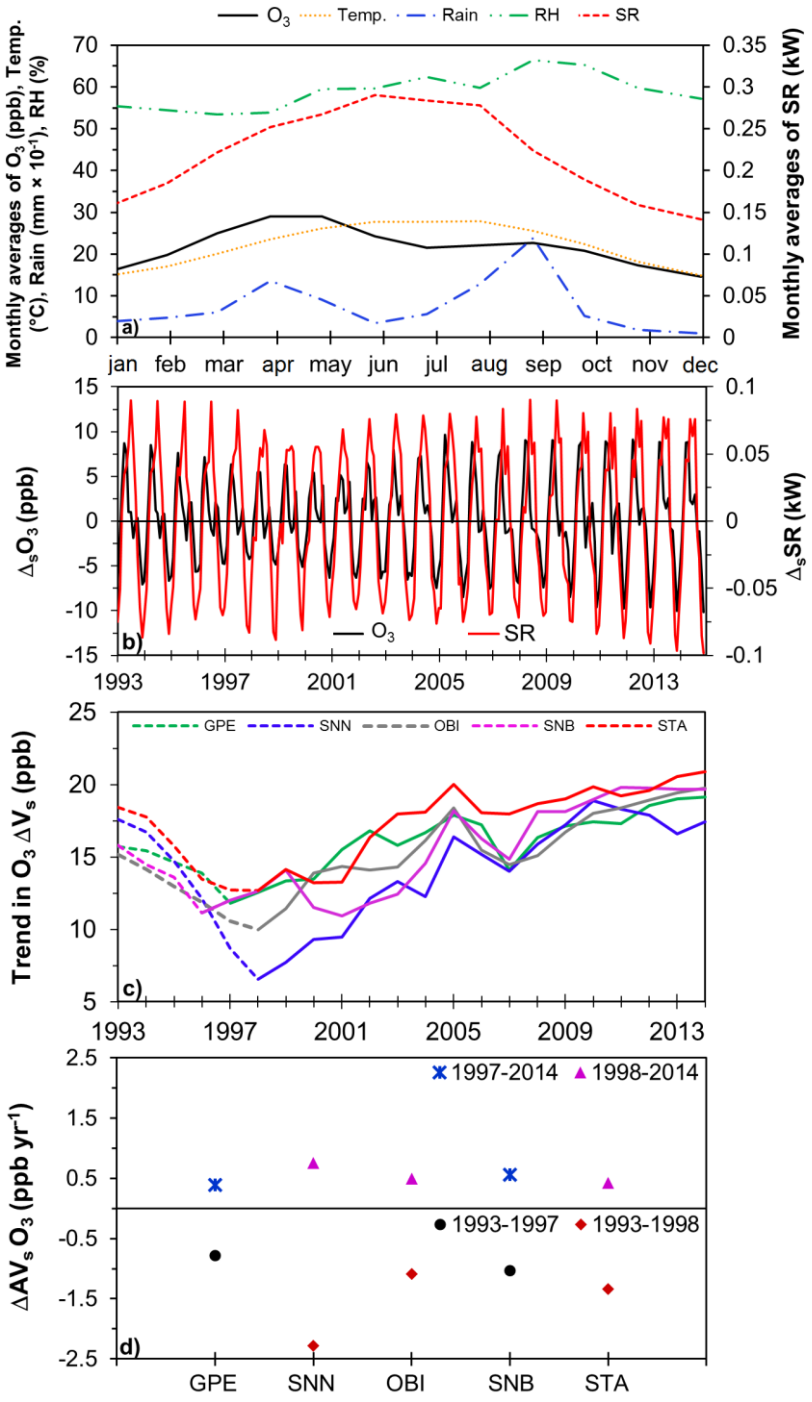

Fig. 8a). Annual cycles of O_3, temp., rain, RH and SR constructed by averaging records from 1993 to 2014 for a 1-year period. **b).** Average seasonal cycles in O_3 and SR within the MMA, constructed from monthly averages filtered with the STL technique developed by Cleveland et al. (1990). **c).** Trends in AV_s of O_3 recorded at the 5 monitoring sites within the MMA from 1993 to 2014. The decline in AV_s observed is due to the economic crisis experienced in Mexico during 1994-1996, followed by persistent increases in AV_s since 1998. **d).** Annual rates of change in O_3 AV_s by site, before and after the 1994-1996 economic crisis.

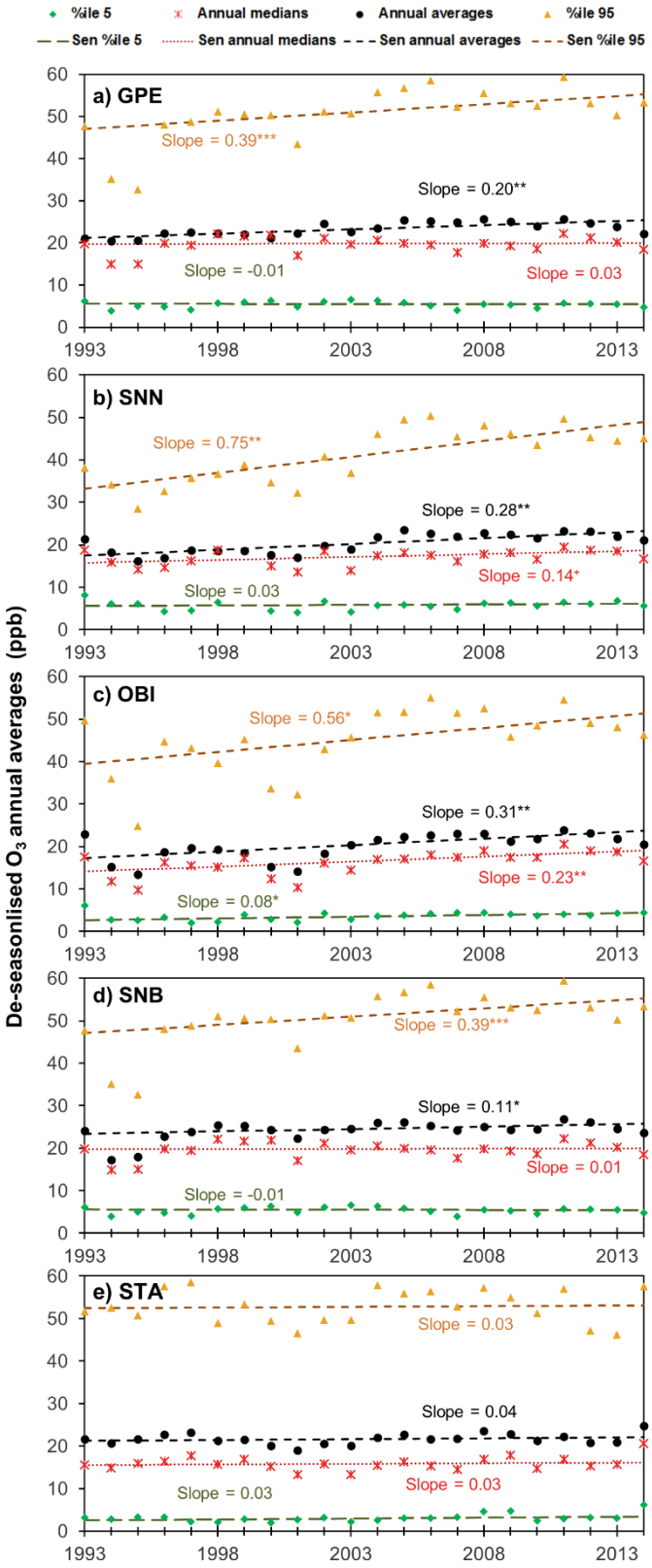

Fig. 9. Long-term trends of de-seasonalised annual O_3 data at the 5th %ile, median, average and 95th %ile, for the 5 sites within the MMA during 1993-2014. The dashed lines represent the Sen slopes. Statistical significance is expressed as p<0.1 = $^+$, p<0.05 = *, p<0.01 = ** and p<0.001 = ***.

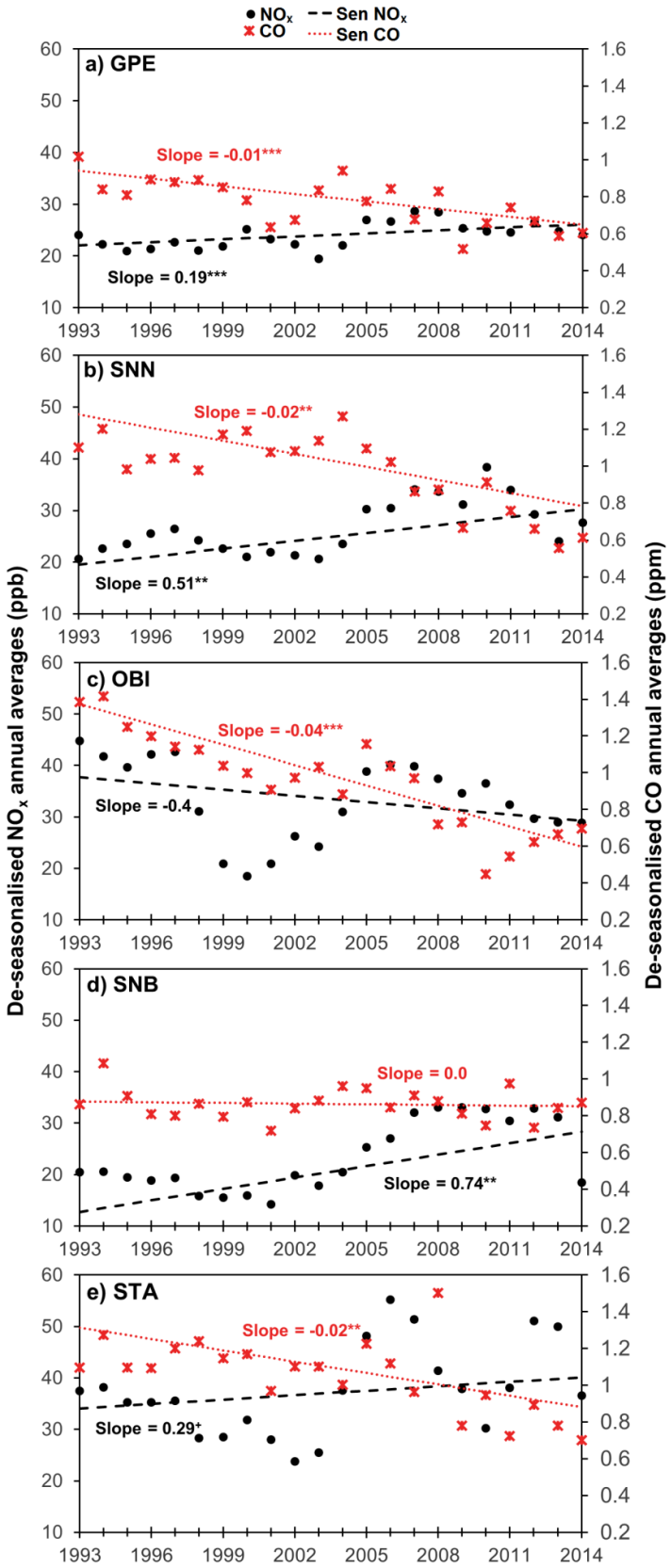

Fig. 10. Long-term trends of de-seasonalised annual averages for NO_x and CO at the 5 monitoring sites within the MMA during 1993-2014. The dashed lines represent the Sen slopes. Statistical significance is expressed as $p<0.1$ = $^+$, $p<0.05$ = *, $p<0.01$ = ** and $p<0.001$ = ***.

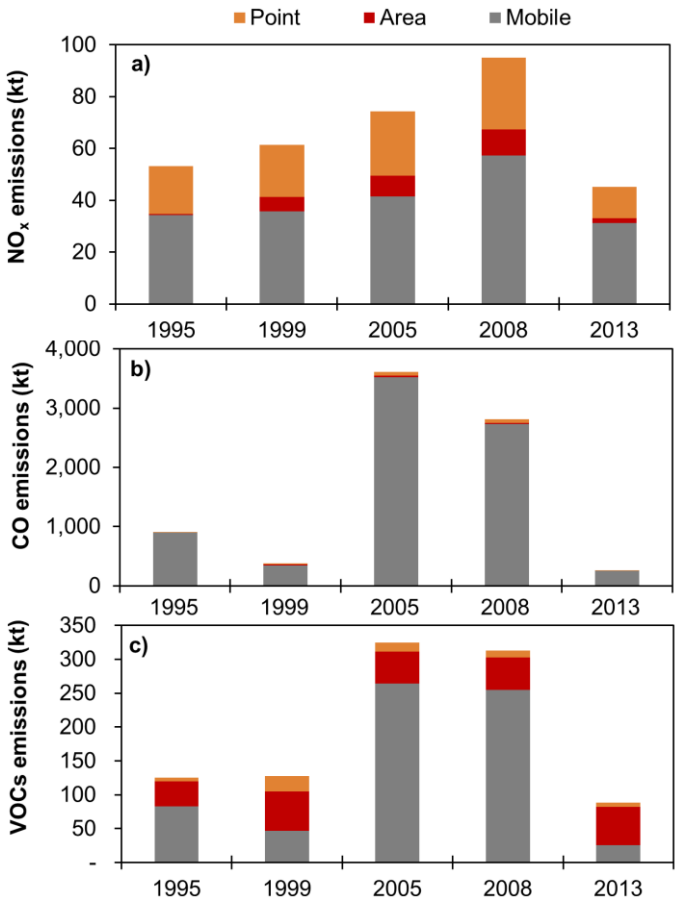

Fig. 11. Emission estimates for anthropogenic NO_x, CO and VOCs within the MMA. The estimates from 1995 and 2013 correspond to State emission inventories and the ones from 1999, 2005 and 2008 correspond to the NEI. (Source: SEMARNAT, 2006, 2011, 2014; SDS, 2015).

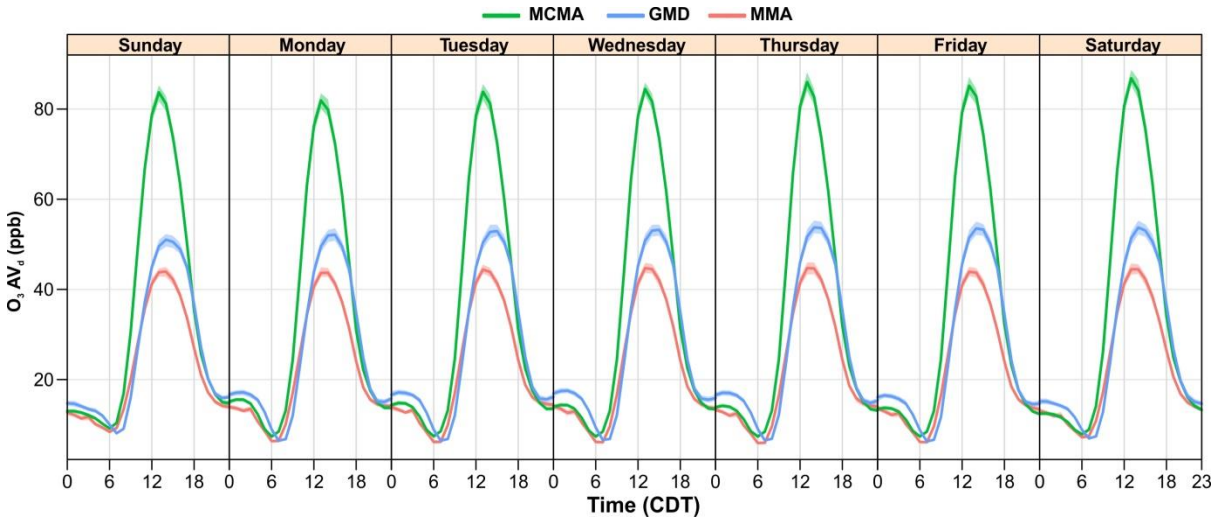

Fig. 12. Average weekly cycles of O_3 at the three major metropolitan areas in Mexico during 1993-2014 for the MCMA and the MMA, and between 1996-2014 for the GMA. The shading shows the 95% confidence intervals of the average.

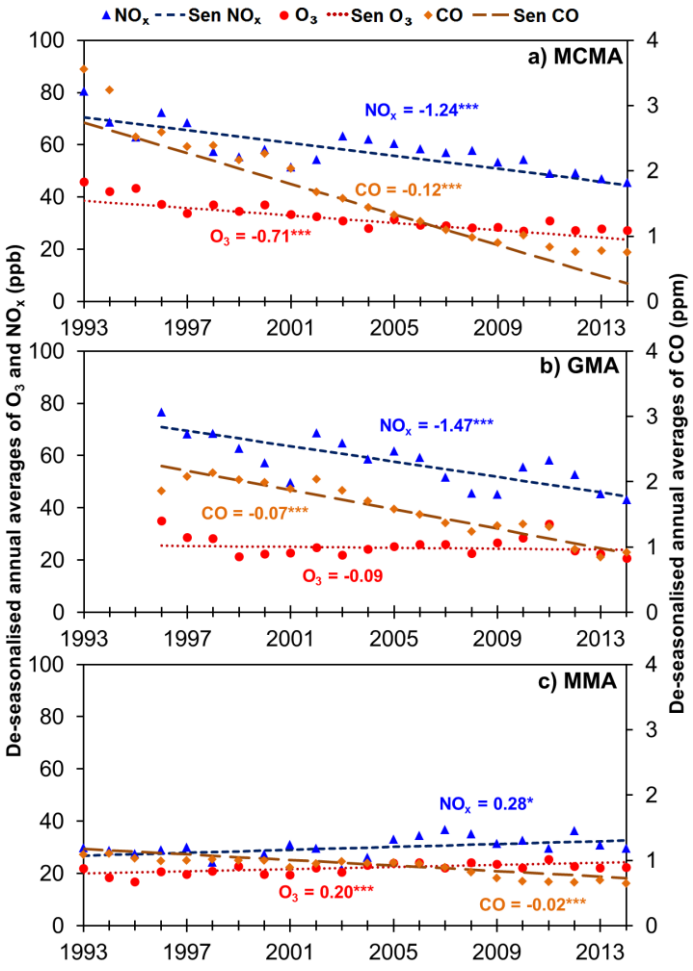

Fig. 13. Long-term trends of de-seasonalised annual averages of O_3, NO_x in ppb, and CO in ppm for the MCMA and MMA during 1993-2014, and for the GMA during 1996-2014. The dashed lines represent the Sen slopes. Statistical significance is expressed as p<0.1 =$^+$, p<0.05 = *, p<0.01 = ** and p<0.001 = ***.

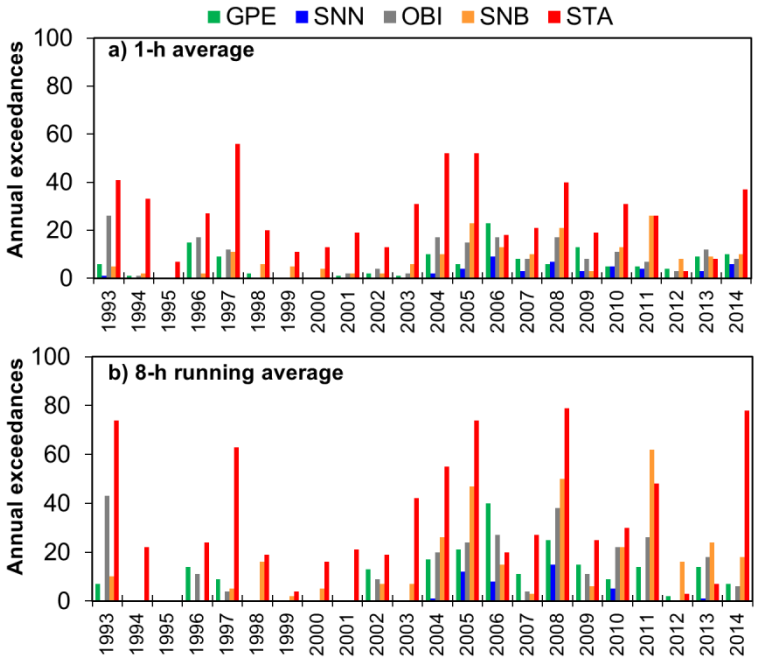

Fig. 14. Annual exceedances of the O_3 NOM for 1-h averages (110 ppb) and 8-h running averages (80 ppb) at the 5 monitoring sites within the MMA from 1993 to 2014.